The Remote Sensing of Tropospheric Composition from Space

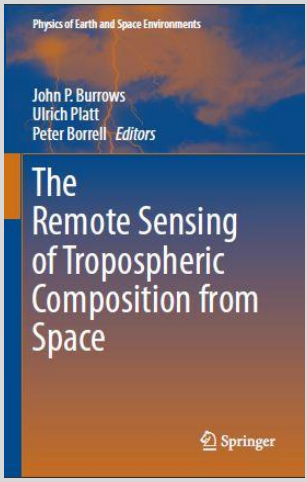

Editors:
John P. Burrows
Ulrich Platt
Peter Borrell

Pages 1 to 66

Chapter 1

Tropospheric Remote Sensing from Space

John P. Burrows, Ulrich Platt and Peter Borrell

Publisher: Springer Verlag, Heidelberg
Springer Book Web Page
Springer on line Page for the Book
ISBN 978-3-642-14790-6
DOI 10.1007/978-3-642-14791-3

February 2011

Chapter 1
Tropospheric Remote Sensing from Space

John P. Burrows, Ulrich Platt and Peter Borrell

1.1 Remote Sensing and the Scope of the Book

The study of the distributions and amounts of trace constituents in the troposphere, using satellite instruments orbiting some 800 km above in space, is a science that has developed within the past twenty or so years and which is having a large influence on both monitoring the global and regional atmospheric environment, and within the research field of atmospheric chemistry. The field is a relatively new scientific discipline within the field of Earth Observation.

Remote sensing is the act of obtaining information about an object from a distance. In the context of our atmosphere, it comprises the detection of changes in electromagnetic radiation reaching the observer and the subsequent determination of the abundance of trace constituents in the atmosphere, such as trace gases, including water vapour, and particles such as aerosols, clouds, smoke and dust.

Our own eyes and ears evolved as remote sensors, and we all use remote sensing when looking at clouds, smoke, dust and hazes. Chemical constituents are not so evident, but used to be seen in the orange plumes of nitrogen dioxide from reactors in chemical factories and, unhappily, from the greenish tinge of chlorine over the battlefields of the First World War. We are able to see, i.e. use remote sensing, through the atmosphere because the principal gases, nitrogen, N_2 and oxygen, O_2, are largely transparent in the visible region of the spectrum.

Remote sensing principally utilizes the interaction of electromagnetic radiation with the trace constituents; thus the absorption, emission and scattering of radiation by molecules or particles results in changes in the spectral or temporal

J.P. Burrows (✉)
Institute of Environmental Physics (IUP), University of Bremen, Germany
and
NERC Centre for Ecology and Hydrology, Wallingford, United Kingdom

U. Platt
Institute of Environmental Physics (IUP), University of Heidelberg, Heidelberg, Germany

P. Borrell
P&PMB Consultants, Newcastle-under-Lyme, United Kingdom

J.P. Burrows et al. (eds.), *The Remote Sensing of Tropospheric Composition from Space*, Physics of Earth and Space Environments, DOI 10.1007/978-3-642-14791-3_1,

characteristics of the radiation. These changes are then interpreted to reveal information about the object.

In the context of this book, remote sensing refers to obtaining information on trace constituents using spectroscopic instruments mounted on satellite platforms. These generally give a global coverage and provide data on global and regional scales.

As indicated below, remote sensing has been extensively used for studying the atmosphere, particularly air pollutants such ozone, O_3, whose existence was discovered by Christian Schönbein (Schönbein 1840), nitrogen dioxide, NO_2, and sulfur dioxide, SO_2 both at ground level and vertically using purpose-built lidar instruments.

In addition, measurements of the global distribution of trace constituents are needed for both environmental monitoring and to test our scientific understanding of the transport and transportation of pollution, air quality and global climate change.

The creation by the governments of the world of the Global Observing System of Systems, GEOSS (GEOSS 2009), which builds on initiatives such as the Integrated Global Observing System, IGOS, is recognition that accurate data is needed by the international policymakers attempting to manage the Earth's resources and control atmospheric pollution from the local to the global scale. Measurements of tropospheric constituents from space will play an important part in this system.

The progress in the remote sensing of the troposphere has been dramatic in the past two decades. The advances have been facilitated in part by technological improvements, the creation of the programmes by space agencies and also by the scientific community through individual work and through national and international projects (Borrell et al. 2003).

So we have moved from an age of scepticism about the value of remote sounding of trace tropospheric constituents from space, to a golden age of first observations and exploitation for science. We are now at the beginning of an age of operational applications and services. The measurements will, we hope, be used to achieve sustainable development delivering an environment having its ecosystem services intact and maximising human well being

The purpose of this book is to describe the state of the art in the field, to explain the technology and techniques used and to demonstrate some key recent findings and results. The book begins in this chapter with an historical perspective of the field together with some the basic physical principles and knowledge required to understand remote sensing from space. The following chapters present the techniques and solutions to the problems associated with the various spectral regions (ultraviolet, visible, infrared, microwave) in which observations are made. Aerosols and clouds, which are covered in the next two chapters, are of particular interest – they not only pose problems for making observations of the lower troposphere from space but they offer intrinsic interest themselves in the fields of climate change, air quality and atmospheric chemistry. Of special importance is the accuracy and reliability of remote sensing data; these issues are covered in a chapter on validation. The final section of the book is concerned with the exploitation of data. There is a chapter on observational results, giving not only results of current interest from

individual studies, but also examples of the use of data from two or more satellites to obtain insights into particular atmospheric environmental problems. A chapter follows on the comparison of global and regional observations with chemistry-transport models and climate models, and the added value that the interaction brings to both. The book concludes by summarising our progress and indicating likely future developments in the field. It also includes suggestions for the actions needed if we are to have the global observation system that the Earth needs to assess its present, deteriorating state.

Also included in the book is a list of satellite instruments used for tropospheric composition measurements (Appendix A), an Atlas with a global view of several complementary parameters useful in interpreting satellite data (Appendix B) and, in Chapter 8, an Atlas of global distributions of most common tropospheric trace substances. This is also accessible as a pull-out section in the rear cover. Appendix C is a list of the abbreviations and acronyms which prevail in this field. Appendix D gives a set of time lines for future missions which highlight the likely gaps in our coverage in future years, unless action is taken soon.

Overall the book is addressed to anyone interested in Earth observation and the details of remote sensing of trace gases, clouds and aerosols, in particular students of the environmental sciences, and scientists working in the field. It gives a timely account of the recent developments in this emerging area, which are proving to be of much utility in the atmospheric environment.

1.2 Earth Observation and Remote Sensing

The science of Earth observation, the study of the Earth and its atmosphere using space-based instrumentation is a new field, of much importance to the modern world. Since the industrial revolution, both the population of the Earth, and its standard of living, have been increasing nearly exponentially, as a result of the availability of low cost energy and materials from fossil fuels. However such activity results in pollution and the growth has resulted in air pollution intensifying on local scales and expanding regionally and globally. Such anthropogenic activity is now changing the conditions in much of the lower atmosphere and at the Earth's surface globally and, it is generally agreed, is changing the state of the atmosphere leading to climate change and global warming.

In order to assess these changes detailed measurements on all scales, both to monitor our changing atmosphere and to test and verify our current knowledge and understanding of the Earth–atmosphere system, are needed, and those from space potentially meet this need on regional and global scales.

Over the last 50 years, remote sensing has developed at a great pace through technical advances in scientific instrumentation, optics and rocketry. The period has seen a pioneering voyage of discovery, and Earth observation has come of age during this period. These advances have been made possible by the ingenuity of mankind, powered by the availability of cheap energy from fossil fuel combustion.

Much public attention has been focused on man's exploration of space, and the greatest use of satellites is probably for military surveillance, communications and television. However the most important outcome of the space age has been perhaps the development of remote sensing techniques for studying our atmosphere. Techniques often developed initially for ground based and aircraft platforms, have been adapted to exploit the unique advantages of the observational geometry available from space, with both passive and active remote sensing techniques being exploited for Earth observation.

Passive remote sensing exploits the measurement and analysis of the electromagnetic radiation coming from the sun and the Earth itself, after it has passed through the atmosphere. In active remote sensing, artificial sources of radiation are used to detect the back scattered radiation and the temporal evolution of changes in intensity.

Examples of parameters or objects, which are targets for Earth Observation include:

- surface colour (vegetation; "land use", ocean colour),
- albedo and/or surface spectral reflectance,
- cloud cover,
- aerosol properties,
- thunderstorms (flash frequency),
- fire parameters,
- surface and air temperature,
- wind velocity and direction,
- ocean waves,
- sea ice,
- column densities of trace gases,
- vertical profiles of trace gases.

The production of meaningful data requires instrument development, data acquisition, retrieval theory, data analysis and interpretation. The results in the geophysical sciences provide "fields", and the goal is to determine these fields and observe their changes in time and space:

- pressure and temperature fields (e.g. meteorology),
- gravity fields (e.g. geophysics, planetology),
- electrostatic fields (e.g. geophysics, planetology),
- electromagnetic fields (e.g. geophysics, geology, geography).

The spatial and temporal variations in the radiation field are measured by sensors yielding the following quantities:

- radiometric parameters for electromagnetic radiation: geophysical calibrated intensities, polarisation etc.,
- spectral dependence of radiometric parameters.

The aim of tropospheric work is to produce column densities and concentration profiles of gases and aerosols. Since the troposphere can only be observed from

space through the stratosphere, then knowledge of the stratospheric components is also needed. In addition, the tropospheric concentrations are directly related to surface sources, both natural and anthropomorphic, and are strongly influenced by air movements, clouds and precipitation. Thus a variety of satellite-based information is needed for a full interpretation of the results.

1.3 Atmospheric Remote Sensing from Space

This section provides some aspects of the programmatic development of remote sensing, together with a short introductory review of some of the most relevant developments in remote sensing in the solar, thermal infrared and microwave spectral regions. These are expanded upon and developed in detail in the subsequent chapters.

A full list of satellite instruments for observing tropospheric chemical composition with solar back-scattered radiation is given in Appendix A.

1.3.1 Pre-Satellite Days

Remote sensing from elevated platforms is not a new concept; such measurements were foreseen by Benjamin Franklin, who, in 1783 as the American ambassador to France and Belgium, observed Montgolfier Balloons flying over Paris and predicted their use for military reconnaissance purposes. The remote sensing of the Earth's surface from above began in the nineteenth century with the first aerial photographs. A little over a decade after the invention of photography, the French photographer Gerard Felix Tournachon (1820–1910) obtained the first aerial photographs over Paris in October 1859. He later used the same technique to map the countryside. The military applications of remote sensing from balloons were recognized immediately with aerial photography being used by the French in 1859 and by the Northern Army under the command of General McClelland in the American civil war.

Following the invention of manned flight by the Wright brothers at the beginning of the twentieth century, aircraft were exploited extensively for civil and military reconnaissance. In addition low spectral resolution spectroscopic methods, including colour photography, enabled different types of surfaces (vegetation, deserts, etc.) to be characterized. Remote sensing of the surface from aircraft and balloon platforms still remains an important element in Earth observation.

Observations of atmospheric trace constituents using remote sensing also have a long history. The aurora borealis has long been a source of curiosity for the Nordic peoples initially being attributed to divine powers (Roach and Gordon 1973; Bone 1991; Brekke and Egeland 1994). The development of our understanding of atomic and molecular spectroscopy in the nineteenth and twentieth centuries enabled the

observation of air glows to be used to retrieve the amounts and abundances of atoms, molecules and ions in the mesosphere and thermosphere. Another early success of ground based atmospheric remote sensing was the discovery of the stratospheric ozone layer: in 1879 Cornu discovered that absorption of solar ultraviolet radiation was occurring in the upper atmosphere and Hartley in 1880 attributed this absorption to O_3.

1.3.2 Some Historical Milestones in Satellite Remote Sensing

In the following some historical organisational milestones are presented, some of which are expanded in the subsequent chapters of this book. In 1947, captured German V2 rockets were modified by the U.S. military to take pictures of clouds from altitudes of 110–160 km. In July 1955, President Eisenhower announced the intention of the United States to launch satellites for earth observation within the International Geophysical Year, IGY. With the launch of Sputnik by the Soviet Union in October 1957 mankind's exploration of space began.

The first American satellite, Explorer 1, was launched into orbit in January 1958 and carried experiments to study the magnetosphere which led to the discovery of the Van Allen radiation belts. July 1958 saw the creation of the US National Aeronautics and Space Administration, NASA, which aimed to study all aspects of the civilian exploration of space. Within the IGY activity, the Vanguard 2 was successfully launched in January 1959 and measured the Earth's albedo. Canada became the third country to launch a man-made satellite into space with the launch of Alouette-1 in 1962, whose payload was used to study the ionosphere.

In these early days, primitive remote sensing payloads were often carried by astronauts in the first satellite missions. The resultant collection of photographs of the Earth and spectrometric measurements, collected by the NASA Mercury and Gemini astronauts, was of pioneering significance. It also led to the development of missions to explore systematically the Earth and its atmosphere from space and in the 1960, resulted in the successful Nimbus series of satellites, and subsequently the NASA Mission to Planet Earth.

In the USA, not only NASA but also the Department of Defence (DOD), and the National Oceanic and Atmospheric Administration (NOAA) developed satellite systems for meteorological applications. NOAA operates two types of satellite systems: geostationary satellites and polar-orbiting satellites. Geostationary satellites constantly monitor the western hemisphere from an altitude of ~36,000 km, and polar-orbiting satellites circle the Earth and provide global information from ~800 km above the Earth. The instruments on board these address the evolving needs to supply data for numerical weather prediction, NWP. In 1994 the National Polar-orbiting Operational Environmental Satellite System (NPOESS), which will be the new generation of low earth orbiting environmental satellites, was created with contributions from DOD, NOAA and NASA. Recently the system has been separated again into independent but complementary parts.

European space activity began in the early 1960s with the formation of ESRO (European Space Research Organisation) and ELDO (European Launcher Development Organisation). In 1975 ESRO and ELDO merged to form ESA the European Space Agency. ESA developed its programmes in Earth Observation for research and operational meteorological purposes. In addition, ESA developed the first European Geostationary satellite, Meteosat, whose operation was transferred to the agency EUMETSAT (European Organisation for the Exploitation of Meteorological Satellites), after its creation in 1986. ESA and EUMETSAT collaborate to provide Europe with explorer and operational meteorological Earth observation missions. The European MetOp series of polar orbiting platforms, complements the Meteosat Second Generation for operational meteorology, and began its operation in late 2006.

The EU has created its Global Monitoring of Environment and Security programme, GMES. GMES has many aims including the provision of an adequate space segment for environmental monitoring. The EU, ESA and EUMETSAT are contributing to GMES. GMES has become Europe's contribution to GEOSS.

In addition to the activities in Europe and USA, the Canadian Space Agency has launched atmospheric constituent monitoring missions as have the Japanese Aerospace Space Agency, JAXA. The Chinese, Indian, and Korean space agencies are also developing instrumentation for atmospheric remote sensing from space.

1.3.3 Tropospheric Remote Sensing Using Back-Scattered Solar Radiation

A full list of satellite instruments for observing tropospheric chemical composition with solar back-scattered radiation is given in Appendix A.

Much of this book describes results and applications from the use of passive techniques in the solar spectral range. The technique of measuring the spectral absorption structures of trace gases was pioneered by Noxon (1975) using a ground based spectrometer, and the first balloon measurements of this type were made by Pommereau, Goutail and colleagues at CNRS (Pommereau 1982; Pommereau and Piquard 1994a; 1994b). A ground based network followed using the same approach. Independently, the Differential Optical Absorption Spectroscopy technique, DOAS, was developed initially for long path active remote sensing measurements in the troposphere (Perner and Platt 1979; Platt and Stutz 2008) and later applied to measurements with ground based, aircraft and satellite borne instrumentation. Long path infrared spectroscopy has also been used under atmospheric conditions to detect species in chambers and outside (Tuazon et al. 1980).

In the first satellite missions, observations of mesospheric emissions and stratospheric trace gases were targeted, an important scientific emphasis being to understand the global behaviour of the upper atmospheric ozone, O_3, and the dynamics of the middle atmosphere. The first measurements of O_3 were made within the Soviet programme, and NASA began a substantial research programme in the early 1970s. One focus for measurements within the Nimbus series of satellites was the use of

back scattered ultraviolet radiation, BUV instruments, to determine the vertical profile and total column amount of O_3. The Solar Backscattered Ultraviolet, SBUV, instrument and Total Ozone Mapping Spectrometer, TOMS were launched together on Nimbus 7 in 1979 (Heath et al. 1973; 1975). Subsequently an improved SBUV called SBUV-2 became part of the NOAA operational meteorological system and a series of TOMS instruments were built and flown by NASA (see Appendix A).

The recognition by Fishman that combining the retrieved vertical profile of O_3, derived from SBUV measurements, with the total O_3 column amount, retrieved from TOMS measurements, could be used to separate tropospheric from stratospheric O_3 (Fishman et al. 1990) for the remote sensing of tropospheric gases. O_3 was the first trace gas to be retrieved in the troposphere from space. The approach was later extended to combine TOMS with information from the Stratospheric Aerosol and Gas Experiment, SAGE, which provided retrievals of aerosol, O_3 and water vapour, H_2O, in the stratosphere and upper troposphere under cloud free conditions.

In Europe, the SCIAMACHY (Scanning Imaging Absorption spectroMeter for Atmospheric CHartographY) concept was developed between 1984 and 1988 by Burrows and colleagues at the Max Planck Institute in Mainz and elsewhere (Burrows et al. 1990; 1995; Bovensmann et al. 1999). In contrast to the NASA instruments, which used selected wavelengths, SCIAMACHY aimed to measure the entire solar spectrum from the ultraviolet to the short wave infrared at a spectral resolution appropriate to the retrieval of the spectroscopic absorptions and emissions of trace gases in the atmosphere (Gottwald and Bovensmann 2010).

SCIAMACHY has a long history, which illustrates the vicissitudes that a satellite instrument must undergo before it is launched. As proposed, SCIAMACHY was to make simultaneous observations of limb and nadir back-scattered and reflected radiation from the atmosphere, as well as solar and lunar occultation, as part of a mission proposed for launch in 1988. As well as exploiting the unique capability of the nadir limb and occultation measurements, the nadir and limb measurement strategy was selected to enable stratospheric and mesospheric amounts of trace constituents, determined in limb, to be synergistically subtracted from the total columns determined from nadir observations. Thus SCIAMACHY was the first instrument intended to study tropospheric trace gas distributions. It was successfully launched on ENVISAT in February 2002 and is continuing to deliver data. Thus nearly 20 years elapsed between the first ideas and the launch.

In the meantime however, in December 1988, in response to an ESA call for instrumentation to measure atmospheric constituents for the second European Research Satellite, ERS-2, the SCIA-mini concept was proposed by Burrows, Crutzen and colleagues. SCIA-mini was a smaller scale version of SCIAMACHY and comprised instruments measuring in limb and nadir the UV visible and near-IR at the top of the atmosphere. SCIA-mini, although selected for investigation, was then de-scoped to make only measurements in nadir viewing geometry, being renamed GOME, Global Ozone Monitoring Experiment (Burrows et al. 1999). GOME was launched on ERS-2 in April 1995. Using the ideas developed for SCIAMACHY, GOME became the first instrument to fly in space, dedicated to the study of the amounts and distributions of tropospheric trace gas constituents.

The OMI instrument, proposed and developed in the Netherlands, was launched as part of the NASA Aura payload in 2004. OMI like GOME is a nadir viewing instrument. An operational follow-on of GOME was selected by EUMETSAT and ESA as part of the MetOp series of platforms in the late 1990s. The first GOME-2 instrument was launched aboard MetOp-A in October 2006 and is continuing to make successful measurements.

A more thorough review of remote sensing of troposphere constituents and parameters using solar radiation is given in Chapters 2, 5 and 6 of this book. Validation of these data products are discussed in Chapter 7 and their use for science explained in Chapters 8 and 9.

1.3.4 Remote Sensing Using Thermal Infrared in the Troposphere

The potential of using thermal infrared (TIR) and microwave radiation emerging from the atmosphere for the measurements of atmospheric parameters was recognised by the pioneers of atmospheric remote sensing. Instruments such as correlation radiometers (e.g. pressure modulators), spectrometers, interferometers and instruments utilising the heterodyne technique at longer wavelengths have all flown successfully aboard space based platforms. During the Nimbus programme the first correlation radiometers were tested in space. The MAPS experiment, launched by NASA and flown aboard the space shuttle in 1984 and again in 1994, successfully measured CO from space in limited duration missions. In 1996 JAXA launched as part of its ADEOS-I satellite, the nadir sounding FTIR instrument IMG. Although the satellite ADEOS-1 failed after 9 months, IMG data were used successfully to retrieve the tropospheric abundance of CO and several other species.

MOPITT proposed in 1988, is a Canadian contribution to the NASA Terra mission. MOPITT was launched in December 1999 aboard NASA Terra and has now made over a decade of measurements of carbon monoxide, CO. The AIRS spectrometer, flying aboard the Aqua satellite, is a spectrometer having, as its primary mission, the retrieval of water, and temperature profiles. AIRS however also retrieves CO and SO_2 in the troposphere.

The Microwave Limb Sounder, MLS, was launched in September 1991 as part of the highly successful Upper Atmospheric Research Satellite, UARS, mission (Livesey et al. 2003). MLS measured temperature, O_3, H_2O, and chlorine monoxide, ClO.

The Michelson Interferometer for Passive Atmospheric Sounding instrument, MIPAS, was launched by ESA on ENVISAT in March 2002. MIPAS is a Fourier transform infrared, FTIR, spectrometer for the detection of limb emission spectra in the middle and upper atmosphere (Fischer and Oelhaf 1996). It observes a wide spectral interval with high spectral resolution. The primary geophysical parameters of interest are vertical profiles of atmospheric pressure, temperature, and the volume mixing ratios of over 25 trace constituents.

The Tropospheric Emission Spectrometer instrument, TES, a high resolution nadir sounding FTIR, was launched on the NASA Aura platform. It has been used to retrieve a variety of tropospheric data products including tropospheric O_3 and NH_3. Solar occultation and limb scanning instruments in the TIR are able to retrieve trace gases in the upper tropospheric region.

The CNES/EUMETSAT instrument IASI is an FTIR instrument which has, as its primary operational objective, the retrieval of vertical profiles of temperature and water vapour. However it has also successfully retrieved tropospheric amounts and distributions of other tropospheric trace gases. In addtion to the thermal emission experiments, there are also solar occultation experiments, which target the upper troposphere and above. The NASA ATMOS experiment aboard the shuttle, which flew several times as part of the ATLAS mission was the first using a FTIR interferometer. The Canadian stand alone SCISAT-1 mission with the ACE instrument, which is also an FTIR interferometer has now been making measurements successfully since is launch in 2003.

Further details of the thermal infrared sounding of the troposphere are provided in Chapter 3. The developments for the measurements of trace gases cloud and aerosol data products in the microwave and sub mm regions are described in Chapter 4. A full list of satellite instruments for observing tropospheric chemical composition with thermal IR radiation is given in Appendix A and with microwave radiation in Chapter 4.

1.3.5 TROPOSAT and AT2

One aspect, often overlooked in the development of large technological projects such as the launch of satellite instruments, is the contributions made by individual scientists to the formulation of the initial scientific needs and ideas, and to the development of the spectroscopic instruments themselves. In the field of the remote sensing of tropospheric composition a user group has been formed to encourage the exploitation of data derived from satellite measurements and to suggest future missions that could or should be mounted.

The TROPOSAT project (Use and Usability of Satellite Data for Tropospheric Research) (Borrell et al. 2003) was initiated within the EUROTRAC framework (a EUREKA Environmental Project) by the editors of this book, in order to foster the development of instrumentation and retrieval algorithms and their validation and the utilization for scientific and operational applications. Initially the project received some modest support towards coordination from ESA. The aim was the exploitation of the space-based measurements of back scattered solar radiation from the atmosphere, using particularly the measurements from GOME and SCIAMACHY. Later, the project was incorporated within the framework of the EU ACCENT network of excellence as ACENT-TROPOSAT-2 (AT2) and was extended to include the utilization of measurements of thermal infrared radiation

and the retrieval of aerosols and clouds. Many of the scientists supporting AT2 have contributed to the development of this book.

1.4 The Atmosphere, Tropospheric Chemistry and Air Pollution

Satellite instruments observe the atmosphere from high above and so knowledge of the structure of the atmosphere is essential to the interpretation of the results. Furthermore the trace constituents observed are part of a complex chemistry involving primary sources, rapidly reacting chemical intermediates, and products which are eventually rained out. In this section an outline will be given of the atmosphere and the chemistry of the troposphere.

1.4.1 The Physical Structure of the Atmosphere

The Earth was formed approximately 4.54 billion years ago. The Earth's atmosphere comprises the thin envelope of gas surrounding the Earth, which is held in place by gravitation. The primordial atmosphere, produced by out gassing from volcanic eruptions and the Earth's surface, had a very different composition to that of the present day, being a reducing atmosphere, quite in contrast to our present day oxidising atmosphere. About 3.8 billion years ago life appears to have started on Earth and, as a result, the biosphere began to change the composition of the atmosphere. Since this time the sun, the Earth's atmosphere and surface comprise a complex system, essential for maintaining our environment and life as we know it.

The bulk constituents of the Earth's atmosphere, molecular nitrogen, N_2, and oxygen, O_2, contrast with those of its nearest neighbours Mars and Venus, whose atmospheres are primarily composed of carbon dioxide, CO_2. The conditions within these atmospheres are effectively closer to an inorganic photochemical equilibrium, compared to the Earth's atmosphere, which is better described as a complex biogeochemical reactor.

The chemical processing within the Earth's atmosphere depends on the conditions in the atmosphere itself and at its surface. The pressure within the Earth's atmosphere obeys the barometric equation and falls off approximately exponentially as a function of height as shown logarithmically in Fig. 1.1.

The atmosphere up to ~120 km can be divided conveniently into four regions of positive and negative temperature gradient, the troposphere (Greek: well mixed region), the stratosphere (Greek: stratified region), the mesosphere (Greek: middle) and the thermosphere (Greek: heated region), as shown in Fig. 1.2. The regions are separated by the tropopause, the stratopause and the mesopause respectively.

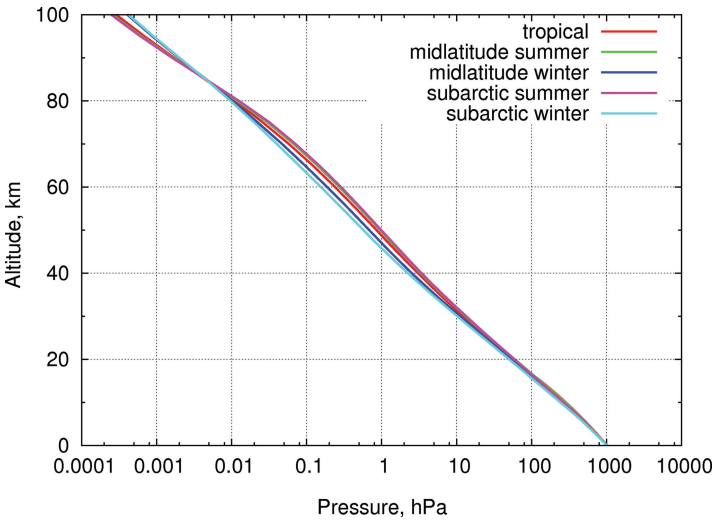

Fig. 1.1 The change in pressure as a function of altitude in the Earth's atmosphere for tropical regions, mid latitudes in summer and winter, and high latitude sub arctic summer and winter. The diagram uses data from the US Standard Atmosphere (1976), and was constructed by J.P. Burrows and S. Noel IUP, Bremen.

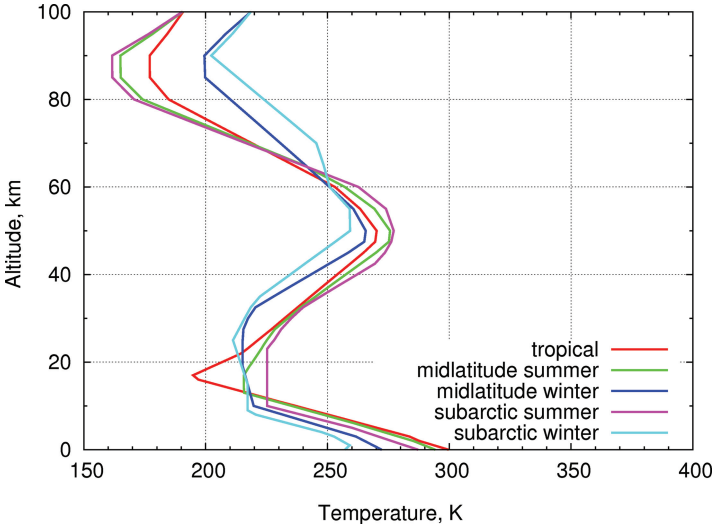

Fig. 1.2 The temperature variation in the atmosphere as a function of altitude for different latitudes and seasons. The regions of the atmosphere having different temperature gradients are: troposphere, below ~12–20 km; stratosphere, ~20 to ~50 km; mesosphere: ~50 to ~90 km; thermosphere, above ~90 km. The diagram uses data from the US Standard Atmosphere (1976), and was constructed by J.P. Burrows and S. Noel IUP, Bremen.

Two regions, the thermosphere and the stratosphere, have positive temperature gradients (or temperature lapse rates) indicating that they are being heated. The thermosphere is the region where short wavelength solar ultraviolet radiation is absorbed by atoms and molecules. Additionally interstellar dust and coronal mass ejections from the sun result in energy and matter being deposited in this region. Photo-ionisation takes place initiating complex physics and chemistry. Overall these processes result in the heating of the thermosphere.

In the mesosphere the photochemistry is considerably less, so the solar warming is diminished and the temperature gradient is negative, as expected from an adiabatic expansion of rising air.

In the stratosphere, which was designated by Teisserenc de Bort and Aßman (1929) the O_2 concentration increases rapidly towards lower altitudes, and absorption by O_2, below about 214 nm in the Schumann Runge bands and continuum, results in O atoms, $O(^3P)$, being formed. These in turn react in a third body reaction to produce ozone, O_3. The O_3 production depends approximately on the square of the O_2 concentration, as suggested by Chapman in 1929 (Chapman 1930). He coupled this with loss of O_3 by photolysis between 220 and 320 nm, and reaction with O atoms to explain the variation of O_3 in the atmosphere as a function of height.

Later it was shown that the reaction of ground state O atoms, $O(^3P)$, with O_3 is too slow to provide the O_3-loss required to bring the model into agreement with observation, but a series of catalytic cycles resulting in an odd oxygen equivalent removal of O_3 in the stratosphere (Wayne 2000) was later identified. The catalytic destruction mechanisms, by which the amount of O_3 is controlled, is complex and have been affected by human activity, namely the tropospheric release of chlorofluorocarbons and bromine-containing species, which are sufficiently long lived to be transported to the stratosphere. As a result of the strong ultraviolet absorption of O_3, the temperature increases in the stratosphere above the tropopause.

The sign of the temperature gradient changes at the tropopause and the region from the surface of the Earth to the tropopause is called the troposphere, which means well mixed. As a result of its negative temperature gradient the troposphere is a region of convective and turbulent mixing; it is this gradient that provides our weather. The lower part of the troposphere is referred to as the planetary boundary layer and is frequently separated from the free troposphere by a further temperature inversion, which has a strong diurnal cycle over land.

Biogenic emissions and most anthropogenic emissions are released directly into the planetary boundary layer; most aircraft emissions are released in the troposphere and the lower stratosphere. These emissions are processed in the atmosphere.

1.4.2 Tropospheric Chemistry

Tropospheric chemistry describes the complex myriad of reactions determining the composition of the troposphere. The chemistry and dynamics of the atmosphere as a whole are complex and coupled. While changes in the extra terrestrial solar

radiation, coronal mass ejections and dust modulate the chemistry and radiation balance in the upper reaches of the atmosphere, the Earth's surface and the planetary boundary layer are the dominant source of bulk and trace constituents for the stratosphere and troposphere (Holloway and Wayne 2010).

Within the troposphere the natural sources of atmospheric constituents (gases and aerosols) include direct release from the biosphere, exchange at the surface, (land, ocean and cryosphere) lightning, natural fires, and stratospheric-tropospheric exchange. Anthropogenic activity, such as biomass burning, the combustion of fossil fuels and changes in land usage, has and is modifying tropospheric chemistry. Figure 1.3a indicates some of the processes diagramatically.

Atmospheric pollution refers to the trace constituents (chemical and aerosol) added to the atmosphere by anthropogenic activity (primary pollutants), and to constituents resulting from the reactions of the primary pollutants in the atmosphere (secondary pollutants). In general during pollution episodes, air masses contain elevated amounts of O_3, aerosol, acids, and other noxious chemical species in comparison with unperturbed air masses. The term *air quality* usually describes the chemical composition of trace constituents close to the surface of the earth, which impact on humans.

Remote sensing of tropospheric composition from space potentially provides global and regional information about the amounts and distributions of key constituents. To use this information to constrain our knowledge of the sources and sinks of atmospheric constituents requires a good knowledge of the chemical processing within the troposphere.

a Free Radical Reactions in the Troposphere

A large part of tropospheric chemistry is associated with the oxidation and subsequent transformation of chemical species released naturally from the biosphere or by anthropogenic activity to the troposphere. Oxidation is often initiated by the attack on a trace substance by the hydroxyl radical, OH, and other free radicals. Hydroxyl is a *free radical*, i.e. a molecule having an unpaired electron, and it is a particularly reactive species. OH can be regarded as the scavenger of the atmosphere, the purpose of which is to remove trace gases and pollutants and so keep the atmosphere clean. OH scavenges hydrocarbons and organic molecules by removing a hydrogen atom to form water. A single simple example is provided by methane, CH_4:

$$OH + CH_4 \rightarrow CH_3 + H_2O \tag{1a}$$

The new species, the methyl radical CH_3, is itself a free radical and reacts immediately with O_2 to form the reactive methylperoxy radical CH_3O_2:

$$CH_3 + O_2 + M \rightarrow CH_3O_2 + M \tag{1b}$$

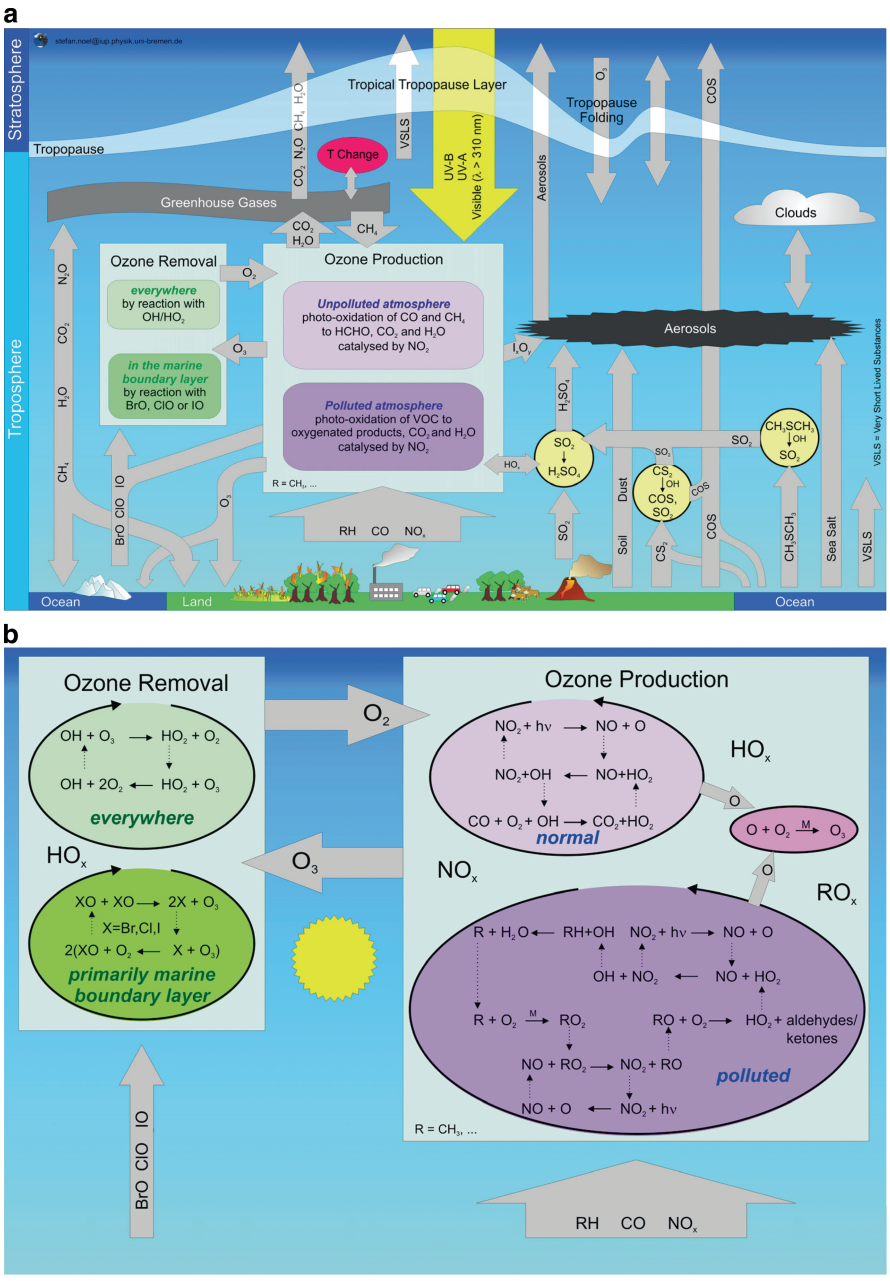

Fig. 1.3 (**a**) A schematic diagram, depicting the complex chemical and physical interactions in the troposphere. The Earth's surface is a natural and anthropogenic source of volatile organic compounds, VOC (also shown as RH), CO, NO_x and other species. Aerosols are produced by physical and chemical processes. Species are removed from the troposphere by deposition to the surface or transport up to the stratosphere. (**b**) An expansion of the boxes in (a) showing some of the chemical processes involved in the production and removal of tropospheric ozone. Figures: J.P. Burrows and S. Noel, IUP, Bremen.

where M is any other molecule. Further reactions then occur generating still more species most of which can react with one another and any other reactive species present. During these processes the OH radical is re-formed so, although it only present at tiny concentrations (mixing ratio of ~10^{-11}), it is always present and active in the daytime atmosphere.

Since virtually all species react with OH, tropospheric chemistry is of much complexity, some of which is illustrated Figs 1.3a and b.

The net result of all the chemical processes in the troposphere is the formation of more stable, oxidised products such as CO_2, organic acids and nitrogen products, which result from reactions involving nitric oxide, NO, NO_2, and many others. These are then removed from the troposphere by both wet and dry deposition or by transport into the stratosphere, where they can be photolysed by UV radiation.

For many trace species of intermediate lifetime, the transport and transformation of longer-lived species represents an important removal process from polluted regions but is simultaneously a source of pollution for pristine regions. These species, of which peroxyacetyl nitrate, PAN, is an example, are termed temporary reservoirs.

Prior to the 1970s the global source of tropospheric O_3 was thought to be transport down from the stratosphere. However, one of the products of the free radical reactions, following further reactions involving NO and NO_2, is the secondary pollutant, O_3. Thus the anthropogenic and natural emissions from the surface to the troposphere result in catalytic cycles (Fig. 1.3b) which, depending on the amount of NO_x, produce or destroy O_3 (Crutzen 1973; 1974). So it is now thought that the greater proportion of tropospheric O_3 is photochemical in origin.

Summer or photochemical smog is a condition where O_3, PAN and other obnoxious trace substances, as well as aerosol precursors, are produced efficiently and locally or regionally in the planetary boundary layer leading to severe pollution under stagnant meteorological conditions (Holloway and Wayne 2010).

A recent development in tropospheric chemistry is the recognition of the importance of chemistry at the boundary between the atmosphere and the cryosphere. Snow and ice interact chemically with gases in the planetary boundary layer. Photochemical reactions in snow (Grannas et al. 2007), result in emissions from the surface. The release of inorganic halogens from ice, in particular bromine (Barrie et al. 1988; Simpson et al. 2007), leads to depletion events for both O_3 and mercury, Hg, in polar regions (Steffan et al. 2008). Release of iodine compounds results in new particle formation and is the subject of much current research (O'Dowd et al. 1998; 2002).

b Stable Species in the Troposphere

The OH radical cannot attack stable oxidised species, so CO_2 produced both by combustion processes and by photochemical oxidation largely remains in the atmosphere, where it has an extremely long chemical lifetime and, since the beginning of the Anthropocene (see below), an increasing concentration. Over land it is removed

by plant photosynthesis and the small signal from the seasonal variation can be seen imposed on the Mauna Loa records, and can be observed from space (see Chapter 8). At the ocean surface, CO_2 participates in an inorganic equilibrium with bicarbonate, HCO_3^-. The net effect is acidification of the oceans and the gradual removal of CO_2.

Another group of compounds unreactive to OH are the chlorofluorocarbons, CFC. These are thus inert in the troposphere and were seen as ideal products for refrigerants, and as blowing agents for plastics. As they don't dissolve appreciably in water, their only fate is very slow diffusion up into the stratosphere; there, they are photolysed into atoms and free radicals which are very active in reducing stratospheric O_3 concentrations. The stratospheric ozone hole, which appears in spring over the Antarctic, leads to increased intensities of surface UV irradiation with deleterious effects on surface ecosystems.

As with CFCs, transport to the stratosphere is the fate of all longer lived species released from the Earth's surface, such as the greenhouse gases, CO_2, CH_4, and nitrous oxide, N_2O. They are mixed by transport, turbulence and molecular diffusion within the troposphere, prior to their exchange to the stratosphere. Once in the stratosphere, they are removed either by photolysis due to the increasing amounts of shorter wavelength solar UV radiation, or reaction with atoms and free radicals, which are more abundant in the stratosphere. The oxidized products are eventually removed from the stratosphere by slow diffusion down to the troposphere and subsequent rain-out.

1.4.3 Air Pollution and Environmental Policy

Perhaps the earliest recorded environmental policy was that of Edward 1 of England in 1306 when he banned the burning of coal in London. The quality of city air remained a matter of public concern over the centuries and was, for example, addressed by Evelyn in "the inconvenience of the aer and smoake of London" in the seventeenth century.

In 1905 the word smog, combining fog and smoke, was coined by Dr. des Voeux to describe the air conditions often observed in large cities. This smog was a characteristic of the boundary layer conditions of London in winter at this time, where the emissions from the burning of coal for domestic heating and industrial processes, coupled with boundary layer humidity, resulted in conditions of low visibility which had adverse health effects. Winter smog, which includes carbon particulates and sulfur dioxide, SO_2, is chemically reducing in character.

A new kind of smog was observed for the first time in the 1950s in southern California, and was termed summer, or photochemical, smog (Haagen-Smit 1952; Haagen-Smit et al. 1952). It is oxidizing in character and also detrimental to health. In the early part of the twentieth century, the population in the region of Los Angeles grew rapidly, as did the large fleet of automobiles. The resultant emissions from transportation and also power generation, coupled with the intense sunshine

(i.e. actinic radiation), the local topography and related local meteorology, yielded particularly favourable conditions for the production of summer smog.

During the past 50 years this type of smog has become an increasingly important environmental issue for urban areas around the globe, particularly in the tropical and semi-tropical regions. While smog control measures have led to reduced pollution in the USA and western Europe, in the summer of 2003 pollution in Europe reached some of the highest levels ever recorded. Severe photochemical smog is now endemic in the vast population centres of developing countries throughout the world.

As a result of global climate change, occasional episodes of pollution, currently considered as extreme, are likely to become more frequent later in the century (Schär and Jendritzky 2004; Schär et al. 2004). The recent attempts to minimise air pollution during the Olympic Games in Beijing (Wang et al. 2009) have further highlighted the potential adverse health effects of photochemical smog, and the drastic measures required to control pollution levels in megacities.

Since the industrial revolution, the rapid growth of the human population and its standard of living has been facilitated by the availability of relatively inexpensive energy, generated in large part from the combustion of fossil fuels. Large changes in land usage have also occurred, where the temperate and tropical forests have been cut or burned down to provide agricultural land. To provide power and to feed the world's population, agriculture has become increasingly intensive. The agrochemical industrial sector now supplies artificial fertilisers, pesticides and other products to the world's agricultural industry on an unprecedented scale. This has resulted in persistent organic pollutants being distributed globally, because they are resistant to environmental degradation through chemical, biological, and photolytic processes. Concern about the global impact of anthropogenic activities on the Earth system has led to the definition of a new geological age, the Anthropocene (Crutzen and Stoermer 2000), which is considered to have begun with the industrial revolution at the end of the eighteenth century.

The research community, initially driven by scientific curiosity, has become involved in quantifying the impact of anthropogenic activity on our environment by both measurement and modelling activities. Comprehensive assessments of our knowledge about ozone, O_3, have evolved since the first concerns about anthropogenically induced destruction of stratospheric O_3 were raised in the 1970s. In agreement with the parties to the Vienna Convention for the Protection of the Ozone Layer and the Montreal Protocol and its amendments on substances that deplete the ozone layer, the WMO, UNEP and their partners now sponsor Ozone Assessments, which appear at four yearly intervals, the latest being the Scientific Assessment of Ozone Depletion: 2006 (WMO 2007); the next one, WMO 2010, is due for publication in 2011.

Twenty years ago, the Intergovernmental Panel on Climate Change, the IPCC, was created by UNEP and the WMO to provide a scientific consensus for policymakers about our knowledge and understanding of climate change. The IPCC publishes specialist reports on topics relevant to the implementation of the United Nations Framework Convention on Climate Change (UNFCCC), an international

treaty that acknowledges the possibility of harmful climate change. The most recent report by the IPCC (2007) confirmed the findings of the previous reports and concluded that there is convincing evidence that climate change is being driven by human activity. The success of the IPCC was recognised in the award of the Nobel Peace Prize in 2007.

The Executive Body of the 1979 UNECE Convention on Long-range Transboundary Air Pollution (LRTAP 2004) established the Task Force on Hemispheric Transport of Air Pollution (HTAP 2007) to develop a fuller understanding of intercontinental transport of air pollution in the northern hemisphere. LRTAP has been important in establishing national and European directives about air pollution. The current debates about the use of agricultural land for the production of bio-fuels and the potential impact of ship emissions are other examples of the challenge facing policymakers in modern times. Overall the assessment process has become embedded in international environmental policy related to air pollution.

1.4.4 Environmental Issues of Relevance to the Troposphere

In the post war period scientific research was linked to the public recognition of a series of environmental issues, which are driven by anthropogenic activity.

(a) Global increase of tropospheric O_3 and degradation of air quality
(b) The transport and transformation of pollution
(c) Biomass burning, and fire
(d) Persistent organic pollutants
(e) Acid deposition
(f) Fine particulate matter with dry diameters smaller than 1, 2.5 or 10 μm, (PM1, PM2.5 or PM10)
To these the following must be added.
(g) Global climate change
(h) Stratospheric ozone depletion, which have tropospheric dimensions

These issues have also led to the recognition of the complex coupling and feedback within the Earth atmosphere system and the need to quantify the mechanisms and processes driving it.

a Global Increase of Tropospheric Ozone and the Effect on Air Quality

Following its discovery in Los Angeles, summer smog is now observed in many urban and rural locations in the northern and southern hemispheres, particularly tropical and sub-tropical conurbations. Emissions from fossil fuel combustion, biomass and waste burning are considered to be the causes of poor air quality. Under typically anticyclonic conditions O_3, aerosols and other toxic compounds can be generated in amounts which are biologically hazardous. The development of the

Asian economies in the past 30 years has been coupled with increasing emissions of a variety of gases and particulate matter. Parts of Asia now have some of the most dramatic episodes of atmospheric pollution and poorest air quality in the world. As noted previously, the heat wave during the European summer of 2003 produced a severe health impact and it is thought that global climate change will result in a higher frequency of such summers in the coming years (Schär et al. 2004).

The recognition of the detrimental effects of smog conditions has led to air pollution and air quality becoming important national and international issues. Air quality addresses the boundary layer condition of air, in particular that experienced close the surface by the biosphere. O_3 is toxic and considered to have negative health impacts at boundary layer mixing ratios above 60 ppb, which is only about 50% higher than the typical mixing ratio observed in summer in Europe. Fine particulate matter is considered to have both short and long term health effects leading to premature death and reduced life expectancy. While at the outset of the 1960s, the troposphere was still perceived to be relatively chemically inactive and globally tropospheric O_3 was considered to originate from the stratosphere and to be removed by dry deposition at the Earth's surface, Crutzen (1973) pointed out that O_3 can be catalytically produced and destroyed in the troposphere. Later analyses of older and more recent measurements indicate a global increase in the amount of tropospheric O_3 (Volz and Kley 1988; Horowitz 2006) by a factor of two to three, with which Models agree (Pavelin et al 1999).

b The Transport and Transformation of Pollutants

As already indicated the importance of transboundary pollution was recognised in the LRTAP Convention (HTAP 2007), and substantial efforts are being made to develop a fuller understanding of intercontinental transport of air pollution in the northern hemisphere. The transport and transformation of pollution around the globe has been recognized in the past decade to be an important part of the anthropogenic modification of the troposphere. For example, in the northern hemisphere, Europe is affected by American emissions, European pollution is transported to the Arctic and Asian pollution to North America. Similarly, in the southern hemisphere, plumes from biomass burning can be tracked from South America to Africa and Africa to Australia.

c Biomass Burning and Fire

Biomass burning and fire has been identified as a potential source of atmospheric pollutants (Watson et al. 1990). Biomass burning and fire are naturally occurring phenomena but there is an increasing anthropomorphic contribution, particularly in the tropics. It is now a major global environmental issue in its own right (Crutzen and Andreae 1990; Levine 1991). Biomass burning is one of the dominant sources for anthropogenic aerosol (Seinfeld and Pandis 1998) and an important source of absorbing aerosol which contributes to warming the atmosphere, thus reinforcing

the effect of greenhouse gases and opposing the cooling effect of most other aerosol species. In addition, fires used for cooking in developing countries contribute to the high concentrations of black carbon with an associated low single scattering albedo.

d Persistent Organic Pollutants

Another important environmental issue relates to persistent organic pollutants, POPs. The United Nations Environment Programme Governing Council started to investigate POPs, beginning with a short list of the following twelve POPs, known as the "dirty dozen": aldrin, chlordane, DDT, dieldrin, endrin, heptachlor, hexachlorobenzene, mirex, polychlorinated biphenyls, polychlorinated dibenzo-*p*-dioxins, polychlorinated dibenzofurans, and toxaphene. Since then, the list has been extended generally to include such substances as carcinogenic polycyclic aromatic hydrocarbons, PAHs, and certain brominated flame-retardants, as well as some organometallic compounds such as tributyltin.

It is unlikely that such substances can be observed directly from space or the ground by remote sensing techniques, as they have low volatility. However knowledge of meteorological parameters, and aerosols as well as biological vectors is required to understand their behaviour. One related example of this general type, is the deposition of mercury, Hg, at high latitudes by a natural process involving halogen oxides.

e Acid Deposition

Acid deposition is a phenomenon of the natural world. Dimethyl sulfide, DMS, and other sulfur containing compounds are emitted by a variety of sources including oceans and volcanoes. These sulfur compounds are oxidised to form sulfur dioxide, SO_2, which reacts in the gas and liquid phases with OH and hydrogen peroxide, H_2O_2, to produce sulfuric acid, H_2SO_4 (Wayne 2000). This has a low vapour pressure and forms cloud condensation nuclei, CCN.

NO_2 reacts with OH to form nitric acid, HNO_3, in the gas phase. The acid anhydride, dinitrogen pentoxide, N_2O_5, formed by the reaction of NO_2 with the nitrate radical, NO_3, readily produces HNO_3 on reaction with H_2O on surfaces or in the liquid phase. HNO_3 has a high solubility in water and, therefore, accumulates in aerosols and cloud droplets, and is rained out.

In an unpolluted atmosphere the natural sources of SO_2 and NO_2 provide a mechanism by which the pH of aerosol and rain are expected to be slightly acidic. In tropical rain forests organic acids produced as a result of biogenic emissions provide a further natural source of acidity.

However, large amounts of NO and NO_2 (together denoted as NO_x) and SO_2 are produced during fossil fuel combustion, which makes the precipitation still more acidic and results in so-called acid rain. In Europe public recognition of the consequences of acid deposition peaked in the middle of the 1980s with the concern

over forest die-back and the acidification of the Scandinavian lakes. This led to the introduction of sulfur scrubbers in the power plants in western Europe.

However acid deposition remains an important environmental issue and research area (Heij and Erisman 1995). Similarly measures, such as catalytic converters in cars, improved design of furnaces in power stations, chemical removal of acid gases, are now also taken to reduce the emissions of NO_x.

f Global Climate Change

Global climate change resulting from man's activity is currently receiving much public attention, having been recognised as a threat to both the biosphere and mankind. Le Treut et al. (2007) have recently provided an interesting review of the development of our understanding of global climate change and greenhouse gases using previous studies by Fleming (1998) and Weart (2003). The first studies of relevance for global climate change date back to the seventeenth century. In the eighteenth century, the mathematician Fourier identified the basic processes of the atmosphere which lead to the greenhouse effect, namely solar radiation is transmitted whereas thermal infrared radiation is absorbed. Tyndall identified the gases CO_2 and H_2O as having this characteristic property, whereas O_2 and N_2 do not. Arrhenius (1896) and others discussed the issue of global warming, caused by the injection of the greenhouse gases such as CO_2 into the atmosphere on a quantitative basis and pondered its impact on glaciers. In the twentieth century progress has been rapid in developing our knowledge of the carbon cycle.

Other gases are often more effective than CO_2, and this has led to the definition of the "global warming potential" of trace gases. The list of greenhouse gases now comprises many species, including water vapour, CO_2, CH_4, N_2O, CFCs and tropospheric O_3. Aerosols have an appreciable effect on the atmospheric radiative balance, as do clouds which have an overall cooling impact that partly compensates for the warming effect of greenhouse gases; however, locally, they are often warming.

The publication of the fourth Assessment Report of the IPCC (2007) and the award of the Nobel Peace prize for 2007 to the IPCC and former USA Vice-President Al Gore for their championing of the issue of climate change has brought an unprecedented but much-needed focus on global warming. The recent assessment of the IPCC has pointed out again the importance of the combustion of fossil fuels as the main driver of global climate change. The United Nations Convention for Climate Change, UNFCCC, has tried to establish targets for reducing emissions but there is still no general international acceptance, even for the necessity of such reductions.

g Stratospheric Ozone Depletion and Its Impact on the Troposphere

A dramatic example of the role of science in the understanding and prediction of an environmental issue was the discovery that stratospheric O_3 is depleted by the

tropospheric release of chlorofluorocarbon compounds, CFCs. Lovelock et al. (1973) made the first measurements of CFCs in the troposphere. Molina and Rowland (1974) then proposed that their presence might lead to a global depletion of the stratospheric O_3 layer in the mid and upper stratosphere. About a decade later large depletions of O_3, measured above the British Antarctic Survey measurement station at Halley in Antarctica, were reported during the Austral spring (Farman et al. 1985). Subsequently the satellite measurements of O_3 from the NASA TOMS and SBUV instruments showed O_3 to be depleted throughout the polar vortex in spring and this behaviour was termed the "Ozone Hole". No atmospheric models had predicted such an effect, because the key chemical processes were not then recognised. During autumn the polar vortex in the lower stratosphere splits off and thereby generates a special set of conditions. The mechanism of the ozone hole formation within the vortex is complex comprising heterogeneous and homogeneous chemical reactions in the lower stratosphere (WMO 2007).

The consequences of a reduction of the stratospheric O_3 layer affect both the stratosphere and the troposphere. In particular the amount of UV-B radiation at the surface and in the troposphere is increased. This biologically damaging radiation also initiates tropospheric photo-oxidation and the generation of tropospheric O_3 is increased. It has been recognized that global warming influences both the intensity and duration of the stratospheric O_3 loss (Shindell et al. 1998; Dameris et al. 1998; WMO 2007). Recently it has been shown that the increasing tropospheric burden of nitrous oxide, N_2O, in the troposphere results from an anthropogenic modification of the Earth's surface environment (Ravishankara et al. 2009). Although the role of N_2O as the source of stratospheric NO_x is well understood, this new study highlights the long term impact of anthropogenic activity changing the surface emission of N_2O. So here is a new aspect of chemistry – climate change – coupling the importance for both the stratosphere and troposphere. In summary, to understand the chemistry of the troposphere accurate knowledge of the following stratospheric parameters is required.

- Stratospheric O_3, which determines the amount of photochemically and biologically active UV radiation in the troposphere.
- Exchange of constituents between the upper troposphere and the lower stratosphere.

These various environmental issues, impacting as they do on local, regional and global scales, are of both national and international importance. To a large extent the issues are the consequence of the higher standards of living and the increase in the world population over the last two centuries and particularly the last 50 years, which is resulting in dramatic changes in the nature of the Earth's surface and increasing emissions of many trace gases to the atmosphere. Management of the anthropogenic influence on global change is a challenging task for the future. Global measurements of key tropospheric constituents are required to be able to attribute appropriately the cause and assess the longer term potential impact of anthropogenic activity on the environment.

1.5 Measuring Atmospheric Composition

Measurements of atmospheric parameters are of central importance for improving our understanding of our atmosphere and environment. However this goal can be achieved in a number of quite different ways. Measurements are characterised by their time scale; i.e. there may be specialised short term measurement campaigns aimed at investigating certain phenomena; on the other hand, long term studies follow the evolution of chemical changes. In addition the spatial scale of the investigation may be local, regional or global. In addition to the measurements made for primarily scientific research purposes, a large number of measurements of atmospheric trace gases are made every day to document the state of the atmosphere, and also to alert the public to extreme pollution events, in order to fulfil legal requirements.

1.5.1 Long Term Observations

Observing and monitoring the changes in atmospheric composition is of great scientific interest. A famous example is the detection of the continuously rising (annual mean) CO_2 mixing ratio directly observed at Manau Loa since 1960 (Keeling et al. 1976; 2003). As the measurement technology has developed, the temporal behaviour of many other important trace gases are now monitored at specific locations around the globe. Long term observations are aimed at monitoring gradual changes in the trace composition of the atmosphere, and include the following trend observations.

- The evolution of tropospheric amounts of CFCs, HCFCs, halons, methyl bromide, and other species which supply halogens to the stratosphere.
- The stratospheric ozone trend.
- The change of stratospheric chemistry (as realised in NDACC).
- The trend in the tropospheric O_3 mixing ratio (GAW).
- Trends in greenhouse gases such as CO_2, CH_4, and N_2O.
- Trends of gases indicating the atmospheric oxidation capacity (i.e. the ability of the atmosphere to remove trace gases). For instance O_3, CH_3CCl_3 or ^{14}CO are monitored for this purpose.
- Trends in aerosol properties.

In this context the “operator dilemma” should be noted: the success of the measurement series hinges on the careful calibration and execution of the measurement procedure over a long period of time. However making the required measurements with the same technique over an extended period of time is often not considered much of a scientific challenge. Thus the psychological side of the project may be as important as the technological aspects in obtaining reliable long term measurements.

1.5.2 Regional and Episodic Studies

Regional and episodic atmospheric studies seek to investigate causes, extent, and consequences of air pollution. While routine monitoring is an issue many fundamental questions can only be investigated by observations made on a regional scale. Typical measurements tasks in this context are:

- monitoring of air pollutants such as O_3, SO_2, NO, NO_2, hydrocarbons, and aerosols,
- investigation of urban plume evolution (e.g. with respect to O_3 formation downwind of source regions),
- mapping of continental plumes,
- observation of the Antarctic stratospheric O_3 hole and
- polar boundary-layer ozone loss events (the "tropospheric ozone hole" (Platt and Lehrer 1996)).

1.5.3 Investigation of Fast In Situ Photochemistry

Studies in smog chambers (also called reaction chambers or photo-reactors) allow of transport processes to be surpressed so that the effect of chemistry alone can be investigated. In fact the phenomenon of tropospheric O_3 formation was observed in smog-chambers long before the chemical mechanism was discovered. The main disadvantage of smog chambers is the presence of surfaces, and so care has to be taken to avoid artefacts, which may arise from chemical processes at the chamber walls. In order to minimise these problems very large smog chambers with volumes exceeding 100 m^3 have been built in recent years, offering surface/volume ratios below 1 m^{-1}.

However, investigation of fast (time scale of seconds) *in situ* chemical and photochemical processes (see Section 2.5) in the open atmosphere allows one to neglect the effect of transport, since transport takes place only at longer time scales. Thus it is possible to study chemical processes directly in the atmosphere. In particular this is true for free radical (OH/HO_2) photochemistry, where the lifetime of the reactive species is of the order of seconds.

1.5.4 In Situ Observational Techniques

A straightforward way to analyse the trace gas composition of the atmosphere is to take a sample of air either in a suitable container for later analysis or inside an instrument. In either case the instrument or sampling apparatus has to be brought to the place in the atmosphere where the measurement is desired. These "*in situ*" measurements come close to the ideal of determining trace gas concentrations at a

"point" in space i.e. usually very close to the instrument. A large variety of measurement techniques for atmospheric trace gases (and other atmospheric parameters) is available; a few examples of *in situ* techniques and instruments are given below.

(a) Gas Chromatography (GC, e.g. for the quantification of organic species).
(b) Chemical Ionisation – Mass Spectrometry (CIMS).
(c) Gas-phase Chemiluminescence (e.g. for the detection of NO_2 or O_3).
(d) Chemical amplifiers for the detection of peroxy radicals.
(e) Electrochemical techniques (e.g. used in ozone sondes).
(f) Matrix Isolation – Electron Spin Resonance (MI-ESR).
(g) Derivatisation – HPLC or Hantzsch reaction (e.g. for aldehyde speciation and detection).
(h) "Bubblers" combined with wet chemical, colourimetric, or ion-chromatographic (IC) analysis.
(i) Photoacoustic spectroscopic detection (e.g. ethene).
(j) Short-path non-dispersive absorption of radiation (e.g. for the measurement of O_3 and CO_2).
(k) Folded-path (either by multi-reflection cell or optical resonator) absorption spectroscopy. This technique comes in many varieties, e.g. using tunable diode lasers or broad-band light sources combined with spectrometers.

In situ techniques represent the traditional approach to study and monitor the atmospheric trace gas composition; their strength is the conceptual simplicity; their main weakness the effort and cost required, in particular when spatial distributions of relatively short lived species (like air pollutants) are to be observed over large areas and over long periods of time. Moreover, *in situ* observations require supporting infrastructure on the ground, which is difficult to obtain in remote areas and over the oceans.

1.5.5 Remote Sensing Versus In Situ Techniques

Remote sensing techniques allow one to detect properties of an object from a distance. Applied to the atmosphere, the trace gas composition can be measure at a point which is remote from the probing instrument. Examples are lidar instruments (see Section 1.12), Multi-Axis DOAS measurements, or observation of trace gas distributions from space. In contrast *in situ* instrumentation (see Section 1.5.4) measures trace gas concentrations (or other parameters) at a particular location. There are a series of applications where localised measurements are desirable, for instance for the determination of strong spatial gradients. Since many trace gases have a strong vertical gradient close to the ground, the observation of these gradients requires measurements that are localised in the vertical dimension. It should be noted, however that *in situ* measurements frequently require relatively long integration times, i.e. they average the concentration over a period t_m of time. As a consequence t_m will average over the distance d_m given by:

$$d_m = t_m \times v_w$$

where v_w denotes the wind speed.

Thus an integration time of 5 min at $v_w = 2$ m/s already translates into a spatial averaging over a distance of $d_m = 600$ m (and more at higher wind speeds). This property of *in situ* measurements is important when comparing them with remote measurements from space, which exhibit spatial resolutions approaching 10 km, and probably less for future instruments. Moreover, space-based remote sensing techniques in principle allow measurements at any point on Earth, including remote continental and marine areas.

1.5.6 The Need for Global Tropospheric Measurements from Space

Most chemical compounds regarded as pollutants, with a few exceptions such as CFCs and HFCs, are present in trace amounts in the natural atmosphere. Anthropogenic activity increases their quantities and changes their distributions. The assessment of the impact and consequences of increasing anthropogenic emissions of trace constituents into the atmosphere is not trivial – because of the inherent nonlinear and complex nature of the processes in the atmosphere, a detailed knowledge of the elementary atmospheric processes is required. Thus the measurement of the composition and changing trends in the amounts and distribution of atmospheric constituents (gases, aerosols and clouds) and meteorological parameters provides the data needed to test our understanding of the biogeochemical cycles within the atmosphere.

For long-lived atmospheric species, such as the greenhouse gases, CO_2, CH_4 and N_2O, measurement stations around the globe provide a monitoring network. The network makes highly accurate measurements, suitable for the assessment of the increasing background amounts. However such networks are sparse. It is now recognised that an accurate knowledge of the regional sources and sinks of both short lived and long lived pollutants is needed, and that this can be provided by a mixture of ground based measurements of different types together with satellite based remote sensing (Barrie et al. 2004).

For short-lived species and species having sources that exhibit variability temporally and spatially, the global measurement of constituents from remote sounding instrumentation aboard orbiting space-based platforms provides a unique opportunity to augment our knowledge of atmospheric pollution and biogeochemical cycling. The challenge for the remote sensing of long lived gases from space is to retrieve data products that have sufficient precision and accuracy to test our current understanding of the sources and sinks of these gases.

The interpretation of satellite observations of tropospheric constituents requires the separation of stratospheric contributions, if they are significant, and must take

into account the changes in radiative transfer created by changes in surface spectral reflectance, the changing burden of aerosols, and the vertical profile of the trace constituents. In this context, constraints from *a priori* climatologies and atmospheric models provide essential information.

A hierarchy of atmospheric models has been developed to simulate the current state of the atmosphere, to predict its future behaviour and to estimate its response to both natural and anthropogenically induced change. As indicated in Chapter 9, using data assimilation to combine model and measurements is playing an increasingly important role in determining the distribution of trace constituents. In the future the coupling of models and measurements from the local to the global scale will be of increasing importance.

1.6 Electromagnetic Radiation and Molecular Energy Levels

Remote sensing and earth observation depend on the interaction of electromagnetic radiation with matter, and the accuracy of the derived data products depends on our knowledge of the interaction of light and matter.

1.6.1 Electromagnetic Radiation

Electromagnetic radiation of different types is distinguished by its wavelength or frequency as shown in Fig. 1.4. The wavelength λ is connected to the frequency ν by the speed of light through a medium

$$c = \nu \times \lambda$$

where c is the speed of light and its value is 2.998×10^8 m/s for vacuum. For air under standard conditions c is about 0.03% smaller.

Figure 1.4 illustrates the range of wavelengths of interest and gives the names for different types of electromagnetic radiation. At very short wavelengths ($\lambda < 30$ nm) the scale begins with γ-radiation and X-radiation. At longer wavelengths the UV and IR ranges bracket the spectral range of visible radiation (ca. 380–750 nm). Near IR and short wave IR radiation (ca. 1 μm wavelength) is then followed by the mid IR and far IR regions. Radiation of even longer wavelength is known as sub-mm wave ($\lambda < 1$ mm), microwave, and radio-wave radiation.

While either wavelength or frequency can be used to characterise electromagnetic radiation, normally the wavelength, λ, in nm, is used in the UV-visible, the wavenumber, $1/\lambda = \nu/c$ expressed in cm^{-1}, is used in the IR and the frequency, MHz/GHz, in the microwave regions.

It is a result of quantum mechanics that some aspects of electromagnetic radiation can be described as behaviour of waves while others can only be understood

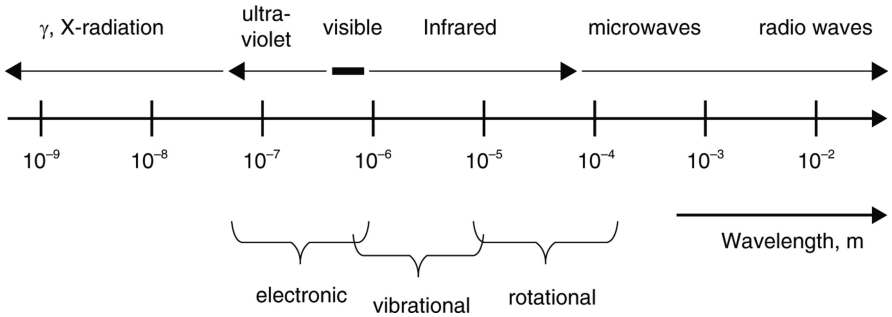

Fig. 1.4 Sketch of the electromagnetic spectrum – γ-rays to radio waves. Also indicated are the types of molecular spectroscopic transitions (electronic, vibrational and rotational) induced by radiation of the respective wavelength ranges. In this book we concentrate on the UV, visible, IR, and sub-mm wave spectral ranges.

when describing radiation as a stream of particles, or photons. The energy E of the photons depends on the frequency (or the wavelength) of the radiation:

$$E = \mathrm{h}\nu = \mathrm{h}c/\lambda$$

where Planck's constant $\mathrm{h} = 6.626 \times 10^{-34}$ Js.

a Scattering and Absorption of Radiation

Electromagnetic radiation passing through a gas may either be scattered or absorbed. When a photon is scattered, the scattering molecule is unaffected but the photon changes direction. Such scattering is known as Rayleigh scattering. The scattering depends on the wavelength of the light and is responsible for the blue skies in the atmosphere (blue light preferentially scattered from light passing above) and red sunsets (red light remaining in the sunlight after losses of blue scattered light).

Scattering also occurs from aerosols, particles and clouds and in this case is known as Mie scattering. Mie scattering depends on wavelength and the particle properties and so can be used to determine aerosol characteristics. Mie theory can be solved exactly for spherical particles. Rayleigh and Mie scattering are examples of elastic scattering (Section 1.9.1).

Rather than scattering the photon of light, the molecule may absorb it; the molecule undergoes an internal change and the energy of the photon promotes the molecule to a higher energy state. Analysis of the interactions, the science of spectroscopy, provides information on the energy states of the molecule normally allowing simple molecules to be easily identified, and their concentrations to be determined.

b Spontaneous Emission, Stimulated Absorption and Emission

Absorption is just one of three processes, identified by Einstein (1917), by which a molecule can interact with radiation while undergoing a change in energy state: stimulated absorption, emission and stimulated emission. These are illustrated in Fig. 1.5.

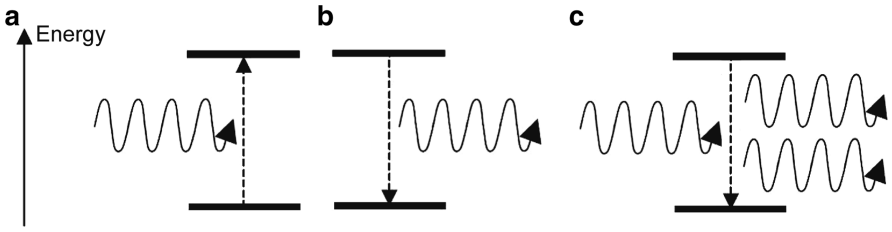

Fig. 1.5 Interaction of radiation with matter: (**a**) stimulated absorption: upon absorption of a photon with the appropriate energy the molecule changes to an excited state; (**b**) spontaneous emission: the molecule returns from the excited to the lower state emitting a photon; this process occurs in fluorescence or phosphorescence; molecules may also lose energy by collision with other molecules; (**c**) stimulated emission: a photon of the appropriate energy interacts with a molecule which is already in an excited state. The molecule is stimulated to return to the ground state emitting a further photon. This coherent emission is the basis of the amplification inherent in laser operation.

- In stimulated absorption, the process already mentioned, a molecule in a lower energy state is excited by the absorbed radiation to an upper excited state.
- In spontaneous emission, a molecule in an upper excited state undergoes a transition to a lower state, losing its energy as an emitted photon of light. This process is the basis of fluorescence and all normally seen light sources.
- Stimulated emission: a molecule, already in an upper excited state interacts with an incoming photon of the correct wavelength and undergoes a transition to a lower energy state so that two photons of the same wavelength are produced. The new photon has the same phase, frequency, polarisation, and direction of travel as the original, so that the radiation emitted is *coherent*. Such a system can act as an amplifier (laser: light *amplification* by stimulated emission of radiation).

Both absorption and emission are used to identify and determine the concentrations of trace species by remote sensing. Stimulated emission is the basis of laser technology used to provide light beams in active systems.

c Raman Scattering

The Raman Effect is a weak interaction of radiation with matter that lies between scattering and absorption. When passing through air, a small fraction of light is elastically scattered, as mentioned above, by Rayleigh scattering, with the scattering molecules remaining unchanged. However a much smaller fraction is also scattered by molecules, which however, undergo an internal transition between energy states. The scattered photon thus has a different energy from the exciting

photon, so that an analysis of this very weak radiation can be used to identify molecules and determine their molecular concentrations. The Raman Effect is an example of inelastic scattering.

Raman scattering, though weak, can provide useful information in passive remote sensing as well as in active systems with intense laser light sources: see Sections 1.9.1 and 1.11.

1.6.2 Molecular Energy States

Molecules, the smallest particle of a chemical compound consisting of chemically bound groups of atoms, are quantum mechanical multi-particle systems. As such their internal energy is quantised and they have discrete energy states. It is the transitions between these states that provide the basis for the interaction with electromagnetic radiation, and the spectroscopic methods by which the molecules can be characterised. There are three molecular energy states which concern us here.

- Rotation of the entire molecule; it is the angular momentum of the entire molecule that gives rise to rotational energy states.
- Vibration of the atoms within the molecule relative to each other gives rise to vibrational energy states.
- The changed configuration of the electrons in the molecule gives rise to electronic energy states.

Typical transition energies ΔE for the different types of transition are:

- Rotational transitions: ΔE of the order of 0.1–1 kJ/mol (or 10^{-3}–10^{-2} eV); the corresponding wavelengths are in the sub-mm or microwave range;
- Vibrational transitions: ΔE of the order of 10 kJ/mol (or 0.1 eV); corresponding wavelengths are in the IR spectral range. Note that a change in vibrational energy will be accompanied by a change in rotational energy, so these transitions may have a rotational "fine structure" when observed;
- Electronic transitions: ΔE of the order of 96 kJ/mol (or 1 eV), corresponding wavelengths are in the visible or UV spectral ranges. Here also a change in electronic energy may well be accompanied by changes in vibrational and rotational energy, so these transitions may well have a vibrational structure with a rotational "fine structure" when observed.

a Rotational Energy Levels and Transitions

Quantum mechanically, the rotational energy levels in a molecule are given by:

$$\mathrm{E_j} = B \cdot J(J+1) \quad \text{with } B = \frac{\hbar^2}{2\Theta} \tag{1.1}$$

where J is the rotational quantum number, B denotes the rotational constant of the particular molecule and rotation mode (rotation axis) with the moment of inertia Θ

with respect to this axis. To a first approximation, Θ is assumed to be independent of J (rigid rotor model). However molecules are not rigid i.e. the atoms within a molecule can change their relative positions (see discussion of vibrational transitions below) due to the centrifugal force leading to a slight increase of Θ at higher values of J compared to its value at low rotational levels. Thus $B \propto 1/\Theta$ will be somewhat lower at higher J values.

Selection Rules for Rotational Transitions

For pure rotational transitions the molecule must have a dipole moment – i.e. an unevenly distributed charge. Then, the difference in the angular momentum quantum number of initial and final state, $\Delta J = \pm 1$, since the photon exchanged with the atom/molecule has a spin (intrinsic angular momentum) of unity. The $\Delta J = -1$ transitions are denoted as P-branch transitions, $\Delta J = +1$ as the R-branch, and $\Delta J = 0$ as the Q-branch where transitions can occur if an electronic transition takes place at the same time, or in Raman transitions. Consequently the photon energy $h\nu = \Delta E$ of allowed transitions is given by the energy difference of two consecutive states:

$$\Delta E_j = E_{j+1} - E_j = B \cdot [(J+1) \cdot (J+2) - J \cdot (J+1)] = 2B(J+1) \ \propto J \quad (1.2)$$

Thus a rotational band (a set of observed transitions) consists of a series of equally spaced lines, the difference between two lines being 2B. The value of 2B is of the order of 10^{-3}–10^{-2} eV (about 242–2,418 GHz or 8.1–81 cm^{-1}), so that wavelengths of photons exchanged in such "purely rotational" transitions occur in the sub-mm or microwave ranges.

The rotational lines which accompany vibrational and electronic transitions have a similar structure.

The energies of rotational states are of the order of the thermal kinetic energy of molecules at room temperature, so that most molecules are rotationally excited under ambient conditions (see below).

b Vibrational Energy Levels and Transitions

Vibrations of molecules can be treated approximately as harmonic oscillations, the energy levels of a quantum mechanical oscillator being given by:

$$E_v = \left(v + \frac{1}{2}\right) \cdot \hbar\omega_0 \quad (1.3)$$

with $v = 0, 1, 2, \ldots$ denoting the vibrational quantum number (vibration level) and $\frac{1}{2}\hbar\omega_0 = \frac{1}{2}h\nu_0$ is the zero-point energy of the molecular oscillator. Thus energies of

different vibrational states are proportional to their associated vibrational quantum number, v. Energies of $\hbar\omega_0$ are of the order of 0.1 eV (~24,000 GHz or 800 cm^{-1}), corresponding to wavelengths in the IR spectral range.

Molecules only absorb in the IR if they have a permanent dipole moment, or if the vibration generates a dipole moment. Thus N_2 and O_2 are not IR active while CO is. Of the three vibrations of CO_2, two are IR active. The selection rule for pure vibrational transitions is $\Delta v = \pm 1$.

In addition to vibrational excitation, a molecule is likely to be rotationally excited at ambient temperatures. Thus each vibrational state splits into a series of ro-vibrational states, and the transitions between states are observed as a series of rotational lines (see Fig. 1.6).

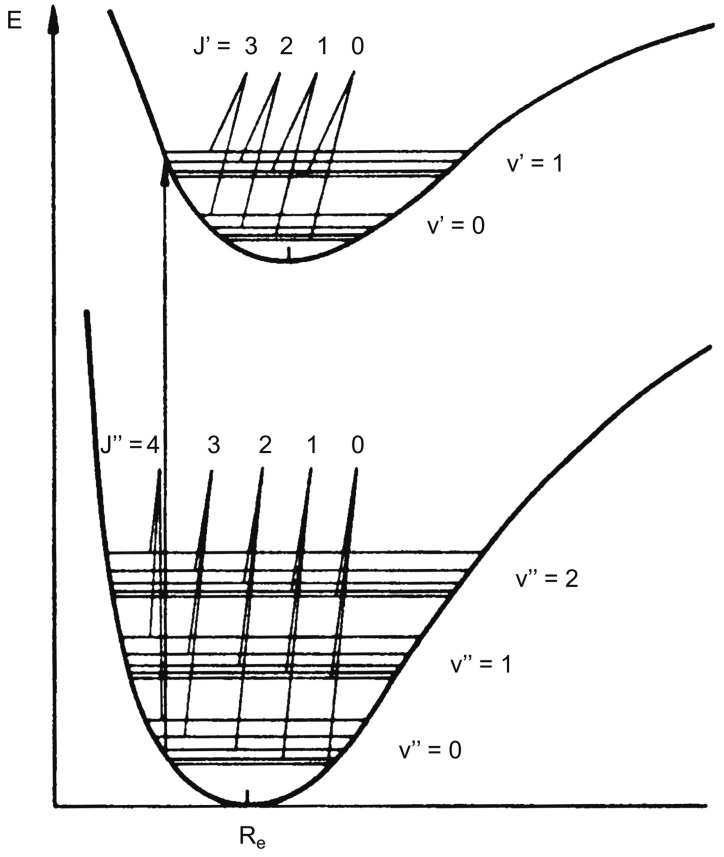

Fig. 1.6 A sketch of the ro-vibrational energy levels (with energy E) of two electronic states of a molecule. Electronic energies are given as function of the distance (R) between the nuclei of the atoms within the molecule, they are at a minimum at a certain distance R_e, which usually differs for the different electronic states. The equidistant, horizontal groups of lines denote vibrational states (ground state: $v'' = 0, 1, 2$, excited state: $v' = 0, 1$) with their attendant lowest rotational levels. Note that the energy separation of the rotational states is exaggerated in comparison to the vibrational energies. (Platt and Stutz 2008).

c Electronic Energy States and Transitions

Electronic energy states result from differing configuration of the electrons in the molecule. Each electronic state has its own set of vibrational and rotational states, these differing from those in the lowest of ground state because both the molecular bond length and strength changes with the electronic configuration.

A potential energy diagram depicting two electronic states in a molecule is shown in Fig. 1.6. The vibrational constant ω, and rotational constant B, can differ in the two states. As a consequence the rotational line spacing in the spectrum is no longer equidistant; rather the lines tend to group towards a certain wavelength either below ("blue shaded" band) or above ("red shaded" band). Electronic states are designated according to their angular momentum (electronic and rotational combined) and their electronic spin. The reader is referred to a spectroscopic text for further details (e.g. Herzberg 1950).

There are no simple selection rules for electronic transitions: the transitions between electronic states are determined by the quantum mechanical characteristics of the respective states. One finds that some transitions are allowed, that for IO in Fig. 1.7 for example. Some are forbidden and so have no spectrum, and some are very weak such as the absorption in the near IR at 762 nm by O_2 itself.

The Frank-Condon principle provides a guide to the intensity of the vibrational transitions for a given electronic transition: during the transition the bond length, or inter-nuclear distance, cannot change, so in terms of the diagram, transitions must be vertical. Since the inter-nuclear distance differs between the states then the observed transitions usually result in a change in the vibrational quantum number.

d The Populations of Molecular Energy States

The population, i.e. the number of molecules in a particular state with energy E, N(E) of different states of a molecule with the energies E_1, E_2 above the ground state (where $E_0 = 0$) as a function of temperature T is given by the Boltzmann–Distribution:

$$\frac{N(E_2)}{N(E_1)} = \frac{G_2}{G_1} \cdot e^{-\frac{E_2 - E_1}{kT}} \tag{1.4}$$

Here k denotes the Boltzmann constant, while G_1, G_2 are the statistical weights or degeneracy factors (i.e. the number of different states with the same energy E) of the respective states. Vibrational excitation in molecules is not degenerate i.e. $G_v = 1$, while rotational states have a degeneracy of $G_J = 2J + 1$, thus the population of rotational states is given by:

$$\frac{N(E_2)}{N(E_1)} = \frac{2J_2 + 1}{2J_1 + 1} \cdot e^{-\frac{E_2 - E_1}{kT}} = \frac{2J_2 + 1}{2J_1 + 1} \cdot e^{-\frac{B(J_2(J_2+1) - J_1(J_1+1))}{kT}} \tag{1.5}$$

With $E(J) = B \times J(J + 1)$, where B is the rotational constant of the particular molecule and rotational axis as given in Eq. 1.1. The kinetic energy of a molecule at room temperature of around 290 K is comparable to or larger than the lowest rotational energy level, but smaller than the lowest vibrational energy level of most molecules. Therefore, under ambient conditions several rotational states are usually populated, but only a small fraction of the molecules are vibrationally excited.

1.7 Molecular Spectra and Line Broadening

An example of an electronic spectrum is provided in Fig. 1.7, which shows the spectrum of the IO molecule. The bands seen are vibrational bands the intensities of which are, as explained above, governed by the Frank-Condon principle.

The rotational structure is not generally resolved, but can indeed be observed under high resolution in some of the IO electronic vibrational bands. As indicated below, the linewidth of the rotational lines is governed by the lifetime of the electronic state. For stable states, the lines are sharp, but for shorter lived electronic states the lines are broader. As will be explained, lines are broadened by pressure and by the Doppler effect.

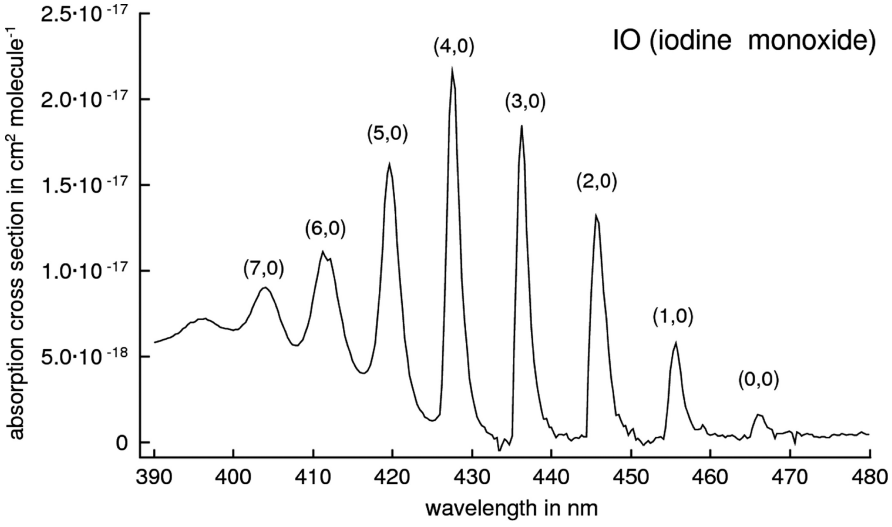

Fig. 1.7 Example of the vibrational structure of the spectrum of IO (electronic transition: $A^2\Pi \rightarrow X^2\Pi$). The bands correspond to transitions to different vibrational levels; the designation (v', v'') gives the vibrational quantum numbers of the upper and lower levels, v' and v''. The rotational fine structure is not resolved. Figure: J.P. Burrows, A. Schoenhardt, J.C. Gomez Martin and P. Spietz, IUP, Bremen.

In general, thanks to the line broadening effects and to the mass of the molecules, only diatomic molecules and a few small polyatomic molecules exhibit resolved rotational structure in their electronic spectrum. Larger molecules usually have continuous spectra. Thus only a limited range of molecules have useful spectra in the UV-visible region and can be detected by satellite instruments. However some of these are the most important environmental species.

In the IR, a greater range of molecules display a rotational fine structure and so thermal IR measurements are useful for a range of molecules that cannot be seen in the UV-visible.

1.7.1 Line Broadening Mechanisms and the Width of Absorption Lines

According to classical electrodynamics, for an excited molecule with energy E_0 above the ground state, the energy of the excited electrical dipole will decrease exponentially with time t as a result of emission of electromagnetic radiation:

$$E(t) = E_0 e^{-\delta t} \tag{1.6}$$

Here δ denotes a damping constant, where $\tau = 1/\delta$ as the time in which $E(t)$ decays to 1/e of E_0. Accordingly the corresponding amplitude of the electric field $\widehat{E}(t)$ of the emitted radiation will decrease exponentially with time t:

$$\widehat{E}(t) = \widehat{E}_0 e^{-\delta t/2} \cdot \cos(\omega_0 t + \varphi) \tag{1.7}$$

Here ω_0 denotes the frequency of the oscillation, which is related to the energy E_0 of the excited state $\omega_0 = 2\pi E_0/h$ (with h = Planck's constant), while φ is the phase of the oscillation. Since the amplitude $\widehat{E}(t)$ is damped, the radiation cannot be truly monochromatic, as can be seen from the Fourier transform of $\widehat{E}(t)$:

$$\widehat{E}(t) = \frac{1}{\sqrt{2\pi}} \int_{-\infty}^{\infty} a(\omega) e^{i\omega t} d\omega \tag{1.8}$$

with the spectral function $a(\omega)$:

$$a(\omega) = \frac{E_0}{2} \left[\frac{e^{i\varphi}}{i(\omega - \omega_0) - \delta/2} - \frac{e^{-i\varphi}}{i(\omega + \omega_0) + \delta/2} \right] \tag{1.9}$$

Since $\delta << \omega_0$ at frequencies ω near the resonance frequency ω_0, we can neglect the second term in the square bracket of Eq. 1.9 and obtain the radiation intensity $I(\omega)$ as the square of $a(\omega)$ (and normalising the integral over $I(\omega)$ to unity):

$$I(\omega) d\omega = I_0 \frac{\delta^2/4}{(\omega - \omega_0)^2 - \delta^2/4} \, d\omega \tag{1.10}$$

Equation 1.10 is known as the Lorentz distribution, its maximum is at $\omega = \omega_0$ while $I(\omega) = 0.5\ I(\omega_0)$ at $\omega = \omega_0 \pm \delta/2$, i.e. δ denotes the full width at half maximum (FWHM) of the distribution.

1.7.2 The Natural Linewidth

The classical image of an oscillating dipole cannot directly be applied to an excited atom or molecule, but the correspondence principle suggests that, at least at large quantum numbers, Eq. 1.10 should be an approximation, with which to describe the profile of an emission line of an isolated molecule, using an empirical δ. In addition there might be more than one level to which an excited molecule can decay: thus $\delta_L = \Sigma\delta_i$ has to be used instead of δ, where the individual δ_i describe the transition frequency to the individual states, to which the excited state under consideration can decay. The natural line shape of an isolated molecule is thus given by:

$$I_L(\omega)\,d\omega = I_0 \cdot \frac{\delta_L^2/4}{(\omega - \omega_0)^2 - \delta_L^2/4}\ d\omega \tag{1.11}$$

with the natural line width δ_L being the FWHM. It essentially depends on the lifetime of the excited state of the molecule, but not directly on the energy difference of the transition and thus the frequency of the emitted or absorbed radiation. For the usual observed transitions the natural lifetime is of the order of 10^{-8} s corresponding to $\delta_L = 10^8$ Hz. For radiation of $\lambda = 400$ nm wavelength ($\omega = 2\pi c/\lambda \approx 4.7 \times 10^{15}$ Hz) this would amount to $\Delta\omega/\omega \approx 2.1 \times 10^{-8}$ or a linewidth, $\Delta\lambda \approx 8.5 \times 10^{-6}$ nm (≈ 0.01 pm). This is usually negligible compared with pressure or Doppler broadening.

1.7.3 Pressure Broadening (Collisional Broadening)

Collisions of the molecules in a gas will reduce the lifetime of the excited state below the value given by radiative transitions alone Eq. 1.10 which determines the natural line width. The shape of a pressure broadened line is Lorentzian, as given by Eq. 1.10 with the width of the pressure broadened line, $\delta = \delta_P$. In principle the collisional damping constant, δ_C, is given by the product of the gas kinetic collision frequency z_{AB} and the deactivation probability p_{AB} per collision. Since p_{AB} can differ for each molecular species, the amount of pressure broadening depends not only on the pressure of the molecular species itself but also on the nature of the other species present. Of particular interest are the self broadening (the species itself is the pressure gas, $p_{AB} = p_{AA}$) and air broadening (species A is occurring as a trace species in air, which is species B). In air, deactivation occurs almost exclusively in collisions between molecule A and air molecules. The collision

frequency is directly proportional to the product of gas density (i.e. pT^{-1} where p is the pressure) and also to the average molecular velocity (and thus to $T^{1/2}$). The expression for the pressure – broadened line width δ_P is then:

$$\delta_P(p,T) = \delta_P(p_0,T_0)\cdot\frac{p}{p_0}\cdot\sqrt{\frac{T_0}{T}} = \delta_0\cdot\frac{p}{p_0}\cdot\sqrt{\frac{T_0}{T}} \tag{1.12}$$

Here $\delta_p(p_0, T_0) = \delta_0$ denotes the pressure broadening at some reference pressure and temperature. Typical values at one atmosphere for pressure broadening of light molecules in the near UV are $\Delta\lambda \approx 1$ pm.

1.7.4 Doppler Broadening

The Brownian motion of the molecules in the atmosphere has two main consequences: pressure broadening and Doppler broadening.

1. The energy E is not only dissipated by radiation but also by collisions with other molecules present in the gas. This effect manifests itself as an increased $\delta_P > \delta_L$, the "pressure broadening" discussed above. Since the effect can be described in terms of a damped oscillation, the line shape is also given by Eq. 1.10.
2. The Doppler Effect will change the frequency ω_0 of the emitted radiation, as a first approximation, to:

$$\omega = \omega_0\cdot\left(1+\frac{v_x}{c}\right) \tag{1.13}$$

where v_x denotes the velocity component of the emitting system along the direction of propagation and c the speed of light. The distribution of an individual component of the velocity $N(v_x)dv_x$ denoting the number N of molecules, where the x-component of their velocity is in the range of v_x to $v_x + dv_x$, is Gaussian (not be confused with the distribution of the absolute value of the velocity, which is given by the Maxwell–Boltzmann distribution). The resulting Gaussian intensity distribution, centred at ω_0, is given by:

$$\begin{aligned} I_D(\omega)\,d\omega &= I_0\cdot\exp\left(\left(Mc^2/2RT\right)\cdot(\omega_0-\omega)^2/\omega^2\right)d\omega \\ &= I_0\cdot\exp\left((\delta_D/2)\cdot(\omega_0-\omega)^2\right)d\omega \end{aligned} \tag{1.14}$$

Here M denotes the molar weight of the molecule and R the universal gas constant. The FWHM of a purely Doppler broadened line is given by:

$$\delta_D = \omega \frac{2\sqrt{2R \ln 2}}{c} \cdot \sqrt{\frac{T}{M}} = \omega \cdot C_D \cdot \sqrt{\frac{T}{M}} \tag{1.15}$$

The constant $C_D = 2\sqrt{2R \ln 2}/c$ has the value of 2.26×10^{-8} (kg/mol)$^{1/2}$ K$^{-1/2}$. For radiation with a wavelength of $\lambda = 400$ nm, at $T = 300$ K and for air (M $\approx$ 0.029 kg/mol) we obtain: $\delta_D/\omega_0 = \Delta\omega/\omega \approx 2.26 \times 10^{-8}$ or a Doppler width of $\Delta\lambda \approx 9 \times 10^{-4}$ nm (about 1 pm).

1.7.5 Atmospheric Spectral Line Shapes in Different Spectral Ranges

The three broadening mechanisms discussed above have very different magnitudes. The natural linewidths are often very small and can only be observed at very low pressures. Pressure broadening and Doppler broadening have line shape described by Lorentzian and Gaussian functions, and so have different dependencies on wavelength (or frequency).

1. For Lorentzian (i.e. natural or pressure) broadening, the half-width is independent of the frequency ω (Eq. 1.10), while Doppler broadening (Eq. 1.15) is proportional to ω.
2. The intensity (or absorption cross section) of a Lorentzian line (Eq. 1.10) decays only with the square of the deviation from the centre frequency $1/(\omega–\omega_0)^2$, so that a large fraction of the total intensity (or total absorption) is in the wings of the line. In contrast, the Gaussian profile (Eq. 1.14) decays exponentially, so that there is little emission (or absorption) in the wings of the line.

Thus the spectral line shape depends on the spectral frequency and atmospheric temperature and pressure. Doppler broadening is usually negligible at low frequencies, i.e. in the microwave and far IR regions; it becomes noticeable in the near IR, and dominates in the short-wavelength UV. In the visible and UV spectral range Doppler broadening is comparable to pressure (Lorentzian) broadening. The resulting line shape, usually called the Voigt shape, is obtained by convoluting the Gaussian and Lorentzian line shapes:

$$I_V(\omega, \delta_D, \delta_P) = \int_{-\infty}^{\infty} I_D(\omega', \delta_D) \cdot I_P(\omega - \omega', \delta_P) d\omega' \tag{1.16}$$

Fig. 1.8 shows a comparison of the three line shapes.

As absorption is the inverse process to spontaneous emission, the equations above also describe the line shapes of atomic or molecular absorption lines, and so the absorption cross section $\sigma(\omega)$ (or $\sigma(\lambda)$) will show the same wavelength dependence as $I(\omega)$ in Eq. 1.16 above.

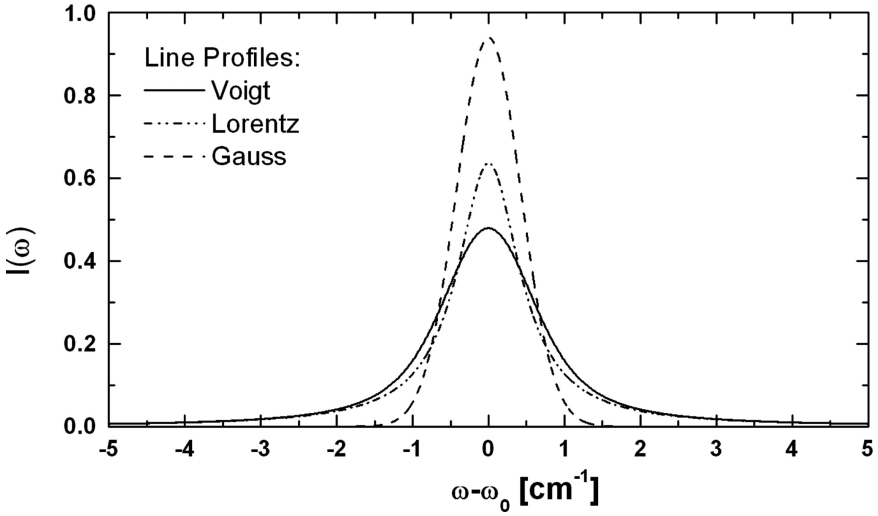

Fig. 1.8 Sketch of the different types of line profiles: Lorentz shape (collision broadening), Doppler (Gaussian) shape (thermal motion of molecules), and Voigt shape resulting from simultaneous Doppler and collision broadening. Platt and Stutz (2008).

1.8 Spectroscopic Techniques for Chemical Analysis

The interaction of radiation with matter provides a powerful tool for a wide variety of investigations, being used for both the investigation of molecular structure and the analysis of the chemical composition of complex mixtures such as are found in the atmosphere. We must first distinguish between two different experimental approaches to spectroscopy.

1.8.1 Absorption Spectroscopy

This spectroscopic technique makes use of the absorption of electromagnetic radiation by matter (Fig. 1.9). Quantitatively the absorption of radiation is expressed by Beer–Lambert law (or Bouguer–Lambert law):

$$I(\lambda) = I_0(\lambda) \cdot \exp(-\sigma(\lambda) \cdot c \cdot L) \tag{1.17}$$

where $I_0(\lambda)$ denotes the initial intensity emitted by a source of radiation and $I(\lambda)$ is the radiation intensity after passing through the medium of thickness L. The species to be measured is present at the concentration (number density) c. The quantity $\sigma(\lambda)$ denotes the absorption cross section at wavelength λ.

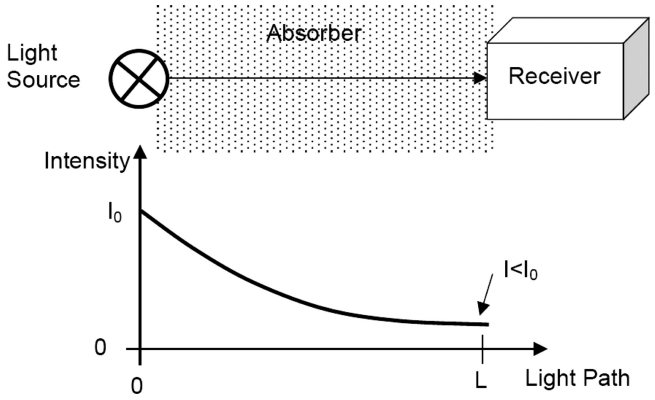

Fig. 1.9 The basic principle of absorption spectroscopic trace gas detection: *top*: an experimental arrangement; *below*: the fall in light intensity as the light passes through the absorber.

The absorption cross section is a characteristic property of any species. $\sigma(\lambda)$ can be measured in the laboratory, while the light-path length L is derived from radiation transport considerations. In the atmosphere, a more general formulation of the Lambert–Beer law involves the column density S:

$$I(\lambda) = I_0(\lambda) \cdot \exp\left(-\sigma(\lambda) \cdot \int c(x) \cdot dx\right) = I_0(\lambda) \cdot \exp(-\sigma(\lambda) \cdot S) \tag{1.18}$$

Once the intensities I, I_0, and the cross section, σ, are known the trace gas concentration, c can be calculated from the measured ratio, $I_0(\lambda)/I(\lambda)$:

$$c = \frac{\log\left(I_0(\lambda)/I(\lambda)\right)}{\sigma(\lambda) \cdot L} = \frac{D(\lambda)}{\sigma(\lambda) \cdot L} \tag{1.19}$$

If L is unknown the column density, S, can be deduced instead:

$$S = \frac{\log\left(I_0(\lambda)/I(\lambda)\right)}{\sigma(\lambda)} = \frac{D(\lambda)}{\sigma(\lambda)} \tag{1.20}$$

The expression:

$$D(\lambda) = \log\left(\frac{I_0(\lambda)}{I(\lambda)}\right) = S \cdot \sigma(\lambda) \tag{1.21}$$

is known as the *optical density* of a layer of a given species (Note that in the definition of the optical density the decadic can be used instead of the natural logarithm; here we shall always use the natural logarithm).

In thermal equilibrium, the emission of any object (solid, liquid, or gas) will be proportional to the Planck function:

$$\mathrm{I}(\nu, \mathrm{T}) = \varepsilon_{\mathrm{x}} \cdot \mathrm{B}(\nu, \mathrm{T}) = \frac{2\mathrm{kc}^2\nu^3}{\mathrm{e}^{\mathrm{hc}\nu/\mathrm{kT}} - 1} \tag{1.22}$$

where ε_x denotes the emissivity of the object, which, by Kirchhoff's law, is equal to the absorptivity of the same object.

1.8.2 Emission Spectroscopy

The spontaneous emission of radiation by excited atoms or molecules is called fluorescence. As the intensity of the emitted radiation is generally proportional to the number of molecules present in a particular volume, emission spectroscopy can be used for the quantitative determination of atmospheric trace gas concentrations. The radiation is emitted at a characteristic set of wavelengths with the photon energy corresponding to the energy difference of the participating states (see Section 1.6). In practice, geometrical factors, the absorption cross section and quenching processes have to be taken into account.

The energy required to transfer the molecule from its ground state to its excited state can be supplied by various mechanisms including collisional excitation. In the TIR and microwave spectral regions, excitation occurs at ambient temperatures in the atmosphere and it is this radiation which is detected by the satellite instruments (Chapters 3 and 4).

Emission spectra in the laboratory can be produced by electron bombardment, chemical reactions, or absorption of radiation. Laser light is a common excitation source in the laboratory and in ground-based observation techniques. Laser induced fluorescence, LIF, is employed in several instruments for the measurement of transient atmospheric trace gases such as the OH radical.

1.9 Atmospheric Scattering and Radiation Transfer

The radiation detected by a satellite instrument has passed from the source, perhaps the sun, to the Earth's surface or a cloud top, through the atmosphere. During the passage some radiation is lost by scattering by molecules or aerosol particles, and some radiation from other sources, also scattered by the atmosphere, reaches the instrument. Thus knowledge of scattering phenomena and the equations for atmospheric radiative transfer are essential in the estimation of trace constituents from space. This section provides a brief introduction.

1.9.1 Scattering

a Rayleigh Scattering

In the atmosphere scattering by molecules and particles is an important process. This is simply demonstrated by looking at the blue colour of a cloud free sky or the white or grey colour of a cloudy sky. Elastic scattering (i.e. scattering without change of the photon energy) by air molecules is called Rayleigh scattering. Another important elastic scattering process, called Mie scattering, is due to aerosol particles (see below). The Rayleigh scattering cross section $\sigma_R(\lambda)$ is given by (Rayleigh 1899):

$$\sigma_R(\lambda) = \frac{24\pi^3}{\lambda^4 N_{air}^2} \cdot \frac{\left(n_0(\lambda)^2 - 1\right)^2}{\left(n_0(\lambda)^2 + 2\right)^2} \cdot F_K(\lambda)$$
$$\approx \frac{8\pi^3}{3\lambda^4 N_{air}^2} \cdot \left(n_0(\lambda)^2 - 1\right)^2 \cdot F_K(\lambda) \quad (1.23)$$

where:

$n_0(\lambda)$ is the wavelength dependent index of refraction of air (real part);

N_{air} is the number density of air (e.g. 2.4×10^{19}molecules/cm^3 at 20°C, 1 atm);

$F_K(\lambda) \approx 1.061$ is a correction for anisotropy (polarisability of air molecules).

However since $n_0(\lambda)^2 - 1 \approx 2(n_0(\lambda) - 1) \propto N_{air}$, $n_0(\lambda) \approx 1$ (e.g. $n_0(550\text{ nm}) = 1.000293$), and $n_0(\lambda) - 1 \propto N_{air}$, $\sigma_R(\lambda)$ is essentially independent of N_{air}. On that basis a simplified expression for the Rayleigh scattering cross section was given by Nicolet (1984):

$$\sigma_R(\lambda) \approx \frac{4.02 \times 10^{28}}{\lambda^{4+x}} \quad (1.24)$$

with $x = 0.04$ (for $\lambda > 550$ nm) and $x = 0.389\lambda + 0.09426/\lambda - 0.3228$ for 200 nm $< \lambda <$ 550 nm.

For simple estimates the Rayleigh scattering cross section can be written as:

$$\sigma_R(\lambda) \approx \sigma_{R0} \times \lambda^{-4} (\sigma_{R0} \approx 4.4 \times 10^{-16}\text{cm}^2\text{nm}^4 \text{ for air}) \quad (1.25)$$

The extinction coefficient due to Rayleigh scattering $\varepsilon_R(\lambda)$ is then given by:

$$\varepsilon_R(\lambda) = \sigma_R(\lambda) \times N_{air} \quad (1.26)$$

The Rayleigh scattering phase function is given by:

$$\Phi(\cos\vartheta) = \frac{3}{4}\left(1 + \cos^2\vartheta\right) \quad (1.27)$$

Taking the anisotropy of the polarisability into account (Penndorf 1957): the above equation becomes

$$\Phi(\cos\vartheta) = 0.7629 \cdot \left(0.9324 + \cos^2\vartheta\right) \tag{1.28}$$

b Raman Scattering

Inelastic scattering occurs if the scattering molecule changes its state of excitation during scattering, a process first identified by Raman. A part of the photon's energy passes from the photon to the molecule to excite either a vibration or rotation or both.

Rotational Raman scattering (RS) only changes the rotational excitation state (Stokes lines, $\Delta J = +2$, S-branch) or vice versa (Anti-Stokes, $\Delta J = -2$, O-branch) ($\Delta v = 0$). If the vibrational state also changes, the term rotational-vibrational RS is used ($\Delta v = \pm 1$). Only discrete amounts of energy given by the energy difference between the excitation states can be absorbed or emitted.

For O_2 and N_2 nuclear spin effects impact on the allowed rotational states and their statistical weighting. A rotational, RS frequency shift of up to ± 200 cm^{-1} occurs. There is also a vibrational shift of $\pm 2{,}331$ cm^{-1} for nitrogen and $\pm 1{,}555$ cm^{-1} for oxygen. The rotational-vibrational RS cross sections are an order of magnitude weaker than the rotational RS cross sections, and the rotational RS, in turn, is roughly one magnitude weaker than Rayleigh scattering.

However, while Raman backscatter from the atmosphere is weak, backscattered radiation from the oceans, rivers and lakes is appreciably enhanced by vibrational RS from liquid water.

c Mie Scattering

Mie scattering (Mie 1908) is defined as the interaction of light with particulate matter with a dimension comparable to the wavelength of the incident radiation. It can be regarded as the radiation resulting from a large number of coherently excited elementary emitters (molecules for example) in a particle. Since the linear dimension of the particle is comparable to the wavelength of the radiation, interference effects occur. The most noticeable difference to Rayleigh scattering is, generally, the much weaker wavelength dependence and a strong dominance of the forward direction in the scattered light.

The calculation of the Mie scattering cross section, which involves summing over slowly converging series, is complicated even for spherical particles; it is worse for particles of an arbitrary shape. However, the Mie theory for spherical particles is well developed and a number of numerical models exist to calculate scattering phase functions and extinction coefficients for given aerosol types and particle size distributions (Van de Hulst 1980; Wiscombe 1980). The computational

effort is substantially reduced by the introduction of an analytical expression for the scattering phase function, which only depends on a few observable parameters. The Henyey-Greenstein parameterisation is most commonly used:

$$\Phi(\cos\vartheta) = \frac{(1-g^2)}{(1+g^2-2g\cos\vartheta)^{3/2}} \tag{1.29}$$

which is only dependent on the asymmetry factor g (average cosine of the scattering function):

$$g = \langle\cos\vartheta\rangle = \frac{1}{2}\int_{-1}^{1} P(\cos\vartheta)\cdot\cos\vartheta \; d\cos\vartheta \tag{1.30}$$

For isotropic scattering (P(cos ϑ) = constant) the asymmetry factor g = 0; for tropospheric aerosol a typical value might be as large as 10.

Tropospheric aerosol is either emitted from the surface (examples are sea salt, mineral dust and soot and particles from biomass burning) or formed in the gas phase by condensation of chemically derived hygroscopic species, principally sulfate, nitrates or oxidized organic material. The physical and chemical properties of aerosols in the atmosphere depends on the aerosol origin and history (see Chapter 6). Parameters for typical aerosol scenarios (urban, rural, maritime, background) can be found in the data base for the radiative transfer model LOWTRAN, (Isaacs et al. 1987), which includes the extinction coefficients and the asymmetry factors as well as their spectral dependence. A radiative transfer model, including all cloud effects known to date, was developed by Funk (2000).

d Total Scattering

Mie scattering is only partly an absorption process but, by similar arguments to those for Rayleigh scattering, it can be treated for narrow beams, such as an absorption process with the extinction coefficient:

$$\varepsilon_M(\lambda) = \varepsilon_M(\lambda_0)\times(\lambda/\lambda_0)^{-\alpha} \tag{1.31}$$

where the Angström Exponent α is inversely related to the mean aerosol particle radius. Typically α is found in the range 0.5–2.5 with an "average" value of $\alpha = 1.3$ (Angström 1929).

In short a more comprehensive description of atmospheric extinction in the presence of a single trace gas species, having a concentration, c, and an absorption cross section, σ, can be expressed as:

$$I(\lambda) = I_0(\lambda)\exp[-L\;(\sigma(\lambda)\times c + \varepsilon_R(\lambda) + \varepsilon_M(\lambda)] \tag{1.32}$$

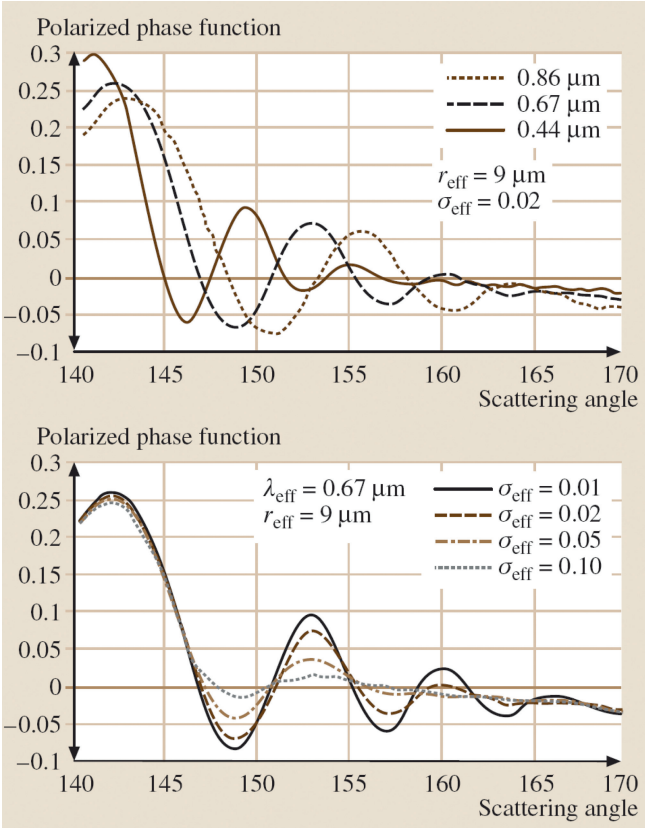

Fig. 1.10 Polarised Mie scattering phase function as a function of scattering angle for cloud droplets having a lognormal particle size distribution with an effective radius r_{eff} = 9µm. Upper panel: phase function as a function of wavelength with fixed σ_{eff} = 0.02 effective size variance; lower panel as a function of effective size variance (adapted from Platt et al. (2007)).

Typical extinction coefficients due to Rayleigh and Mie scattering in the UV at 300 nm are 1.3×10^{-6} cm^{-1} and $1–10 \times 10^{-6}$ cm^{-1}, respectively. In the IR Rayleigh scattering can usually be neglected. Fig. 1.10 shows the Mie theory scattering function for polarised radiation as a function of scattering angle. With an appropriate selection of scattering angle the polarisation information can be used to retrieve information about particles and aerosols.

1.9.2 Atmospheric Radiative Transfer

Radiation transfer in the atmosphere is an important area of scientific study for several reasons.

- Atmospheric radiation transport is central to quantifying the greenhouse effect and thus climate change.
- Atmospheric radiation transport determines the efficiency of photochemical reactions in the Earth's atmosphere.
- Most importantly for this book: the retrieval of trace gas, aerosol or cloud parameters from remote sounding experiments requires an accurate knowledge of the sources of electromagnetic radiation and its transport through the atmosphere.

Accurate radiative transfer models are needed to invert tropospheric trace constituent data products. In the following we describe the physical processes described in radiative transfer. In practice, radiative transfer models are complex and usually require numerical integration, as the resulting system of equations cannot be solved analytically. Monte Carlo methods can be used but remain computationally expensive, preventing their routine use at this stage.

Consider a stream of photons travelling through the atmosphere. The radiant flux, Φ, per unit space angle, Ω, and wavelength, λ, i.e. the incoming intensity I_λ(Eq. 1.33) is attenuated within the distance, ds, by absorption and scattering. The subscripts for the absorption, a, and scattering coefficients, s, are used where the respective coefficients are $\varepsilon_a(\lambda) = n \times \sigma_a(\lambda)$ and $\varepsilon_s(\lambda) = n \times \sigma_s(\lambda)$; n is the number of absorber or scatterers per unit volume and $\sigma_i(\lambda)$ are the absorption or scattering cross sections; they consist of contributions from all the scattering species. The sum of absorption and scattering is commonly referred to as the extinction. The continuity equation for the intensity of the incoming radiation traversing the distance, ds, for a single species is then:

$$dI_\lambda = -[\varepsilon_a(\lambda) + \varepsilon_s(\lambda)] \cdot I_\lambda \cdot ds = -[\sigma_a(\lambda) + \sigma_s(\lambda)] \cdot n \cdot I_\lambda \cdot ds \tag{1.33}$$

ε_a = absorption coefficient,
ε_s = scattering coefficient,
$\sigma_a(\lambda)$ = absorption cross section of the absorbing molecule,
$\sigma_s(\lambda)$ = scattering cross section of the absorbing molecule,
n = number of absorbers/scatterers per unit volume.

There are three primary sources of radiation in the atmosphere: external radiation from the sun (or other celestial bodies), thermal emission by molecules in the atmosphere or from the ground, and scattering, i.e. the radiation removed from the primary beam due to scattering (Eq. 1.33) reappearing as a radiation source. The outgoing light receives some intensity, $dI_{s,\lambda,}$ by scattering from all angles, θ and φ. We introduce a dimensionless scattering function $S(\theta, \varphi)$:

$$S_\lambda(\vartheta, \phi) = \frac{4\pi}{\sigma_s} \cdot \frac{d\sigma_s(\lambda)}{d\Omega} \tag{1.34}$$

which we integrate over all angles weighted with the incoming intensity $I_{s,\lambda,}(\theta, \varphi)$

$$dI_S(\lambda) = \varepsilon_s(\lambda) ds \int_0^{\pi} \int_0^{2\pi} I(\lambda, \vartheta, \varphi) \cdot \frac{S(\vartheta, \varphi)}{4\pi} d\varphi \cdot \sin\vartheta d\vartheta \tag{1.35}$$

to obtain the intensity added to the outgoing intensity dI_s.

The intensity due to thermal emission, $dI_{th}(\lambda,T)$, from the volume element, $dV = A \times ds$, is added to the outgoing intenstity:

$$dI_{th}(\lambda, T) = \varepsilon_a(\lambda) \cdot I_p(\lambda, T)\, ds = \varepsilon_a(\lambda) \cdot F_p(\lambda, T) \cdot A\, ds \tag{1.36}$$

where $F_p(\lambda,T)$ is the flux of radiation at wavelength λ through the area A and, as before, ε_a denote the absorption coefficient and $I_p(\lambda,T)$ the Planck function respectively:

$$dI_p(\lambda, T) = \frac{2hc^2}{\lambda^5} \cdot \frac{d\lambda}{e^{hc/\lambda kT} - 1} \tag{1.37}$$

Combining all the processes above, we obtain the radiation transport equation:

$$\begin{aligned} \frac{dI(\lambda)}{ds} &= -[\varepsilon_a(\lambda) + \varepsilon_s(\lambda)] \cdot I(\lambda) + \varepsilon_a(\lambda) \cdot I_p(\lambda, T) \\ &\quad + \varepsilon_s(\lambda) \int_0^{\pi} \int_0^{2\pi} I(\lambda, \vartheta, \varphi) \cdot \frac{S(\vartheta, \varphi)}{4\pi} d\varphi \cdot \sin\vartheta d\vartheta \end{aligned} \tag{1.38}$$

In general the radiation transport Eq. 1.38 cannot be solved by analytical methods, and numercial modelling is required. However simplifications are frequently possible. For example at short wavelengths (UV-vis) the Planck term can usually be neglected so that:

$$\frac{dI(\lambda)}{ds} = -(\varepsilon_a(\lambda) + \varepsilon_s(\lambda)) \cdot I(\lambda) + \varepsilon_s(\lambda) \int_0^{\pi} \int_0^{2\pi} F(\lambda, \vartheta, \varphi) \cdot \frac{S(\vartheta, \varphi)}{4\pi} d\varphi \cdot \sin\vartheta d\vartheta \tag{1.39}$$

Similarly Rayleigh scattering and Mie scattering by aerosol particles can be neglected for thermal infrared radiation, due to its long wavelength. If there are no clouds (i.e. in the absence of any scattering) we have:

$$\frac{dI(\lambda)}{ds} = \varepsilon_a(\lambda) \cdot \big(I_p(\lambda, T) - I(\lambda)\big) \tag{1.40}$$

With the definition of the optical density $d\tau = \varepsilon_a(\lambda) \cdot ds$ Eq. 1.40 simplifies to:

$$\frac{dI(\lambda)}{d\tau} = I_p(\lambda, T) - I(\lambda) \tag{1.41}$$

This equation is also known as Schwarzschild equation. Even further simplification, i.e. setting the thermal emission to zero ($I_p(\lambda,T) = 0$) leads to:

$$\frac{dI(\lambda)}{ds} = -\varepsilon_a(\lambda) \cdot I(\lambda) = -c \cdot \sigma_a(\lambda) \cdot I(\lambda) \tag{1.42}$$

or

$$\frac{dI(\lambda)}{I(\lambda)} = -c \cdot \sigma_a(\lambda) \cdot ds \tag{1.43}$$

Integration of Eq. 1.43 (taking $\ln(I_0)$ as integration constant) over distance L yields the Beer–Lambert law, Eq. 1.17. Thus the Beer–Lambert law can be identified as the most simple solution of the radiation transport equation.

In Chapters 2 to 6 the particular approaches and simplifications used to solve the atmospheric radiative transfer equation in the different spectral regions are discussed.

1.10 Remote Sensing: Images and Spectroscopy

Using the knowledge of the interactions of electromagnetic radiation with matter and molecular spectroscopy as described above, remote sensing systems can provide data products about atmospheric constituents and surface parameters. The essential components of any remote sensing system comprise the following:

- radiation source (passive: sun, moon, Earth, stars or active: laser, Lamp etc.);
- radiation path (e.g. the atmosphere);
- object (e.g. trace gases in the atmosphere or the Earth's surface);
- sensor (e.g. spectrometer, scanner, radiometer, camera).

1.10.1 Satellite Images

The development over the last 25 years of solid state detector devices and the improvements in fibre optics have revolutionised remote sensing. The modern image sensors determine the spatial distribution of the radiation intensity (radiance) in only one wavelength band, i.e. they produce monochromatic images. Colour image sensors determine the spatial distribution of the radiation intensity in a small number (typically three) of wavelength bands which are typically those corresponding to the human eye's colour impressions, red, green, and blue. An example is shown in Fig. 1.11, which shows a volcanic plume from Etna. However, such images often contain spectral information from UV and IR sensors outside the visible region, and are thus false colour images.

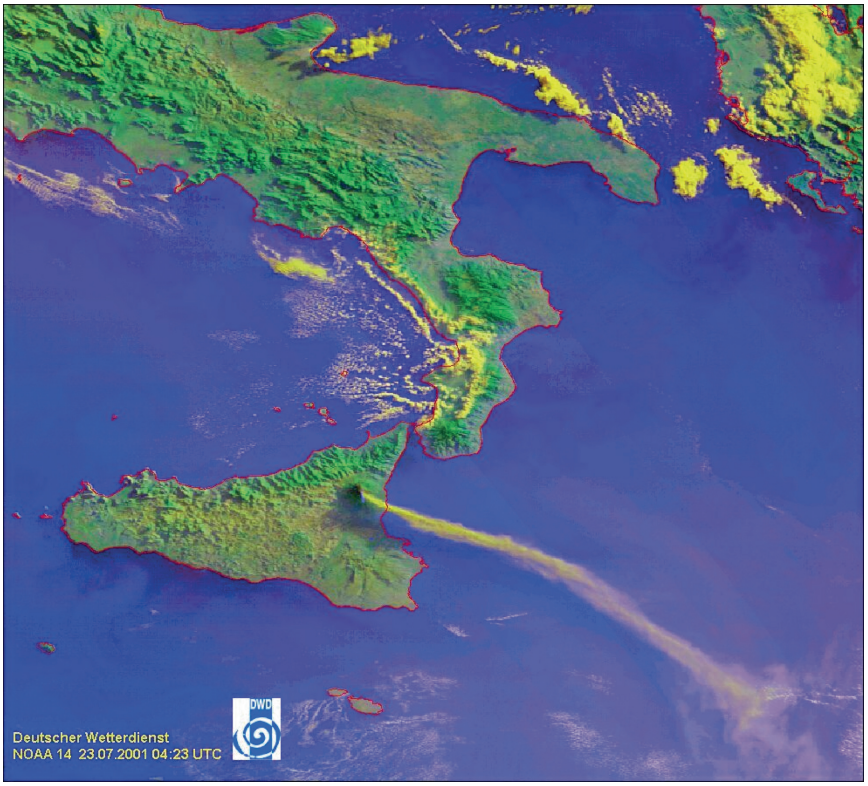

Fig. 1.11 Smoke plume of the Etna volcano – Outbreak on 23rd July 2001.
Source: DWD, NOAA.

Multi-spectral images, such as those used for vegetation detection, are produced by a Hyper-Spectral Scanner. An example of the different reflectivities of various types of ground cover in the spectral range of 400–2,600 nm is given in Fig. 1.12.

Using hundreds or thousands of wavelength intervals, trace gas column densities can be evaluated, for example using DOAS, and reproduced as images. Many examples of this type of image are found in the later chapters of this book.

1.10.2 Spectroscopic Techniques in Remote Sensing

No single spectroscopic technique fulfils every need so that, for a particular application, the technique selected will be based on the particular task to be performed. Questions to be answered in selecting a method are: which species are to be measured; is the simultaneous determination of several species necessary; what is the required accuracy, time resolution, horizontal and vertical resolution?

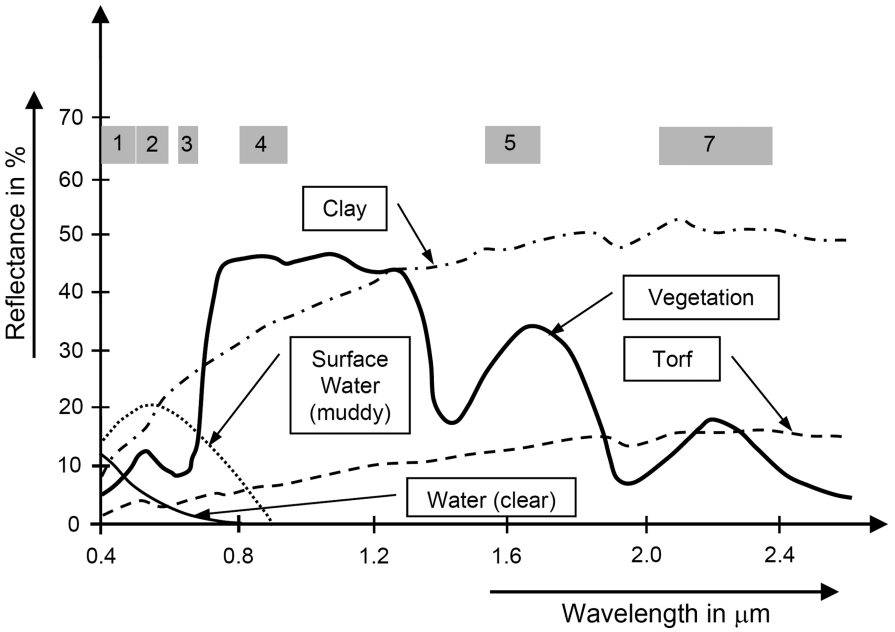

Fig. 1.12 Reflectivity of various ground covers and river water in the spectral range of 0.4–2.6 μm. *Gray*, *numbered boxes* denote the spectral position of the Landsat-TM channels.

Spectroscopic techniques can be broadly divided into methods relying on absorption of radiation directed to the sample from some source, and into spectroscopic analysis of radiation emitted by the sample itself (see Section 1.8).

a Microwave Spectroscopy

Spectroscopy in the mm and sub-mm wavelength range can, in principle, be used in active and passive configurations. To our knowledge detection of atmospheric gases with active microwave instruments (i.e. with instruments employing their own radiation sources) are not currently made, with the exception of water vapour which can be retrieved with the use of GPS signals, see Section 4.8. However measurements of atmospheric parameters (clouds, precipitation, and turbulence) with active radar techniques are common.

Sensors measuring the thermal radiation at mm and sub-mm wave are mostly applied to the quantification of stratospheric species, the technique registering the thermal emission due to rotational transitions of the atmospheric molecules [Janassen et al, 1993]. Many minor atmospheric constituents have emission lines at mm and sub-mm wavelengths. These lines are dominated by pressure broadening which is much larger than Doppler broadening. An upper limit for the profile occurs at an altitude where the pressure and Doppler broadening become comparable.

Since Doppler broadening is frequency dependent, low frequencies are suitable for measuring mixing ratio profiles at higher altitudes. Transitions at mm waves yield the profile well into the mesosphere, examples being O_3, water vapour and CO. At low altitudes the lines become very broad so the present sensor technology limits the profile retrieval to altitudes above 10 km. Observations using the limb sounding geometry yield profile information down to the upper troposphere. Microwave radiometers also provide information on total water vapour, liquid water content and for ice clouds (see Chapter 4).

Measurements by passive microwave and sub-mm wave emission are mostly applied to the quantification of stratospheric species, the technique registering the thermal emission due to rotational transitions of the atmospheric molecules (Janssen 1993). Taking the chlorine monoxide, ClO, molecule as an example, it radiates at $\nu_o = 649.448$ GHz (wavelength: 0.46 mm; $18_{1/2} \rightarrow 17_{1/2}$ transition of ^{35}ClO) (Klein et al. 2002). The line width is dominated by collisional (pressure) broadening, which strongly dominates Doppler broadening ($\Delta\nu_D/\nu_0 \approx v_{molec}/c \approx 10^{-6}$). While the strong variation in line-width with pressure, and thus with the altitude of the absorbing molecule, allows the retrieval of vertical profiles from a thorough analysis of the recorded line shape, it also limits the detection sensitivity to atmospheric pressures exceeding a few mbar. Thus for ClO the best sensitivity is reached in the upper stratosphere, while detection at lower stratospheric or upper troposphere is difficult.

The microwave and sub-mm wavelength range is presently not used for measurements of trace gases in the mid or lower troposphere, due to the large pressure broadening and strong absorption. It is however used in limb and for the retrieval of H_2O and other parameters (see Chapter 4).

b IR Spectroscopy

This spectral range is characterized by thermal emission from the Earth's atmosphere and the ground and encompasses the interval from approximately 3.5–30 μm. In addition, IR solar occultation is employed to probe the upper troposphere and above. Modern IR spectrometers are based on FT techniques and are able to measure a large number of species relevant to atmospheric chemistry, such as CO, CO_2 and O_3 (see Chapter 3).

In the TIR, the averaging kernel (i.e. the region to which the measurement is sensitive, see Chapter 3) depends on the temperature difference between the atmosphere and the Earth's surface. If this difference is low, as in the lower troposphere, there is then little sensitivity and the information content in the observation is primarily in the middle and upper troposphere.

An advantage offered by TIR, as well as microwave and sub mm regions, is that passive operation is not restricted to daylight and observing can continue in the Earth's shadow. Thus one can obtain double the number of measurements from the satellite instrument. Furthermore it is possible to study atmospheric chemical processes in the absence of daytime photochemistry.

c UV/Visible/Short-Wave IR Absorption Spectroscopy

This region encompasses the UV spectrum from about 300 to 400 nm, the visible range (400–700 nm) and the IR range from 700 to about 2,400 nm (2.4 μm). Stratospheric absorption by O_3 precludes observation of the troposphere at shorter UV wavelengths.

The basic optical arrangement is shown in Fig. 1.9. A light source, the reflected light from the Earth, and a receiving system are separated by the vertical extent of the atmosphere. The strength of the technique in this region lies in good specificity and sensitivity for a series of species relevant to atmospheric chemistry and climate. The absence of thermal emission in this range simplifies the radiation transport calculation appreciably (see Section 1.9). A particular advantage is the potential for high sensitivity throughout the atmosphere including the atmospheric boundary layer. In particular, at relatively long wavelengths such as the short wavelength IR, the sensitivity allows the precise determination of total column amounts of important greenhouse gases such as CO_2 and CH_4, with relative errors typically below 1%.

The normal mode of observation is passive, but active techniques have the potential to combine the advantages of the passive approach with the capability of providing altitude-resolved measurements and measurements in the absence of daylight. Two techniques have been proposed: (a) the use of artificial light sources on the ground, and (b) aerosol lidar and Differential Absorption Lidar (DIAL) on satellite platforms (see Section 1.12.2). While lidar techniques in space look promising for the determination of trace gas profiles, only aerosol lidar instruments have so far been deployed (see Chapter 6).

1.10.3 Passive and Active Remote Sensing

A schematic description of active and passive remote sensing scenarios is illustrated in Fig. 1.13 and active and passive remote sensing are discussed in more detail below.

1.10.4 Nadir, Limb and Occultation Views

For passive remote sensing, the viewing geometry is a defining parameter and enables particular aspects of atmospheric composition to be probed. There are basically three viewing geometries being used, which are shown schematically in Fig. 1.14.

a Nadir view

Looking down from space towards the nadir direction or close to it, the sunlight reflected from the Earth's surface and the atmosphere (called the "earthshine" in

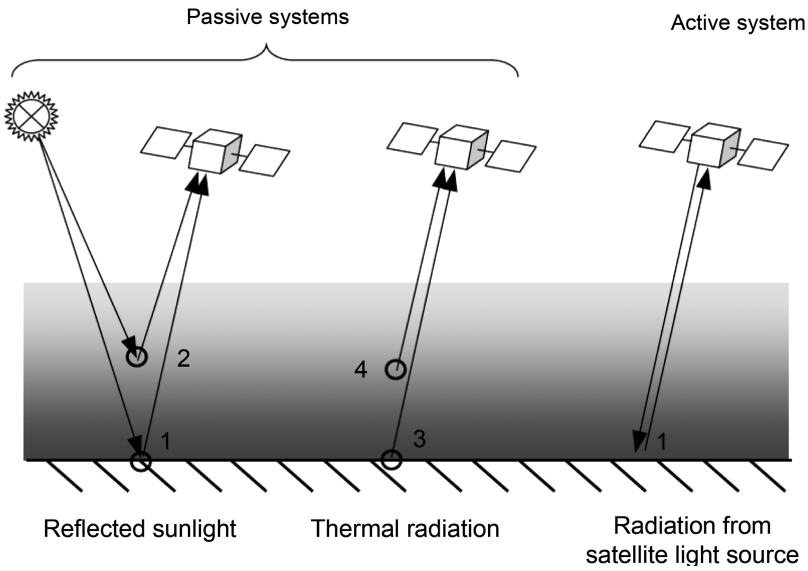

Fig. 1.13 Active and passive remote sensing systems. Possible pathways of the radiation from source to object and sensor are shown. Direct solar radiance can be reflected from the Earth's surface (1), or scattered in the atmosphere (2). Long-wave radiation is emitted from the Earth's surface (3) or from atmospheric gases (4). In summary all processes lead to a modification of the information content.

analogy to "moonshine") is utilised to obtain information on atmospheric trace gas column densities. In this geometry the radiation observed from the atmosphere originates from either the sun, back-scattered from the Earth's surface and the atmosphere or, from the thermal emission in the Earth's surface and atmosphere, or from emissions within the atmosphere. Examples of satellite instruments using this geometry include, for solar measurements: TOMS, SBUV, SBUV-2, GOME, SCIAMACHY, GOME-2 and OMI for UV/vis/NIR spectra, and for thermal IR measurements: MOPITT, TES, IASI. See Appendix A for a full list of satellite instruments.

b Multiple Views

Instruments with several viewing directions offer, in addition to the nadir view, the advantage of multiple paths through the atmospheric boundary layer, which is especially useful for aerosol retrieval. Not only is the AOD higher along a longer atmospheric path, thus providing an extra constraint to the retrieval results but, in particular, the additional view(s) provide a means to eliminate the effect of the reflectance of land surfaces which often dominates the total reflectance. Only a few instruments have more than one view over a particular pixel: (A)ATSR, POLDER/

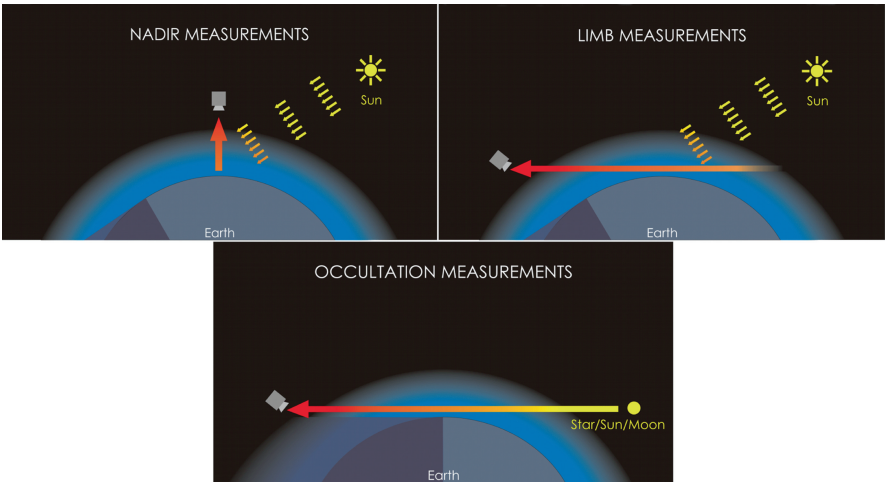

Fig. 1.14 A schematic representation of nadir, limb and occultation viewing geometries used by SCIAMACHY. Figure: J.P. Burrows and S. Noel, IUP, Bremen.

PARASOL and MISR. Hence these instruments provide more constraints on the path radiance and surface effects. In addition to this decoupling of the surface effects, the multi-view instruments can also provide information about the aerosol phase function (Martonchik et al. 1998), and the height of aerosol plumes (Kahn et al. 2007; 2008).

c Limb Mode

In this geometry light scattered from the Earth's rim is analysed. By observing the limb at different tangent altitudes vertical trace gas concentration profiles can be inferred (see Fig. 1.14). Examples of satellite instruments using this geometry include SCIAMACHY, CLAES, ILAS, MLS, ACE-FTS, and OSIRIS. See Appendix A.

d Occultation

By observing the light of the rising or setting sun, moon, or stars through the atmosphere at different tangent altitudes, vertical trace gas concentration profiles can be deduced. Examples of satellite instruments using this geometry include SCIAMACHY, GOMOS, ACE-FTS, HALOE, SAM-II, SAGE-I,II,III, and OSIRIS. See Appendix A.

1.10.5 Active Techniques

In contrast to passive remote sensing which uses the sun, moon, stars and the Earth and its atmosphere as the source of radiation, active remote sensing instruments illuminate the object of interest with a radiation source as part of the instrument. A particular example, which has been used on satellites, is lidar (Rothe et al. 1974; Hinkley 1976; Svanberg 1992; Sigrist 1994). In principle short pulses of a strong, collimated light source, typically from a pulsed laser, are emitted into the atmosphere. By analyzing the temporal evolution of the intensity back-scattered from the atmosphere, the spatial distribution of scattering and extinction along the direction of the emitted (and received) radiation can be determined; this is illustrated in Fig. 1.15.

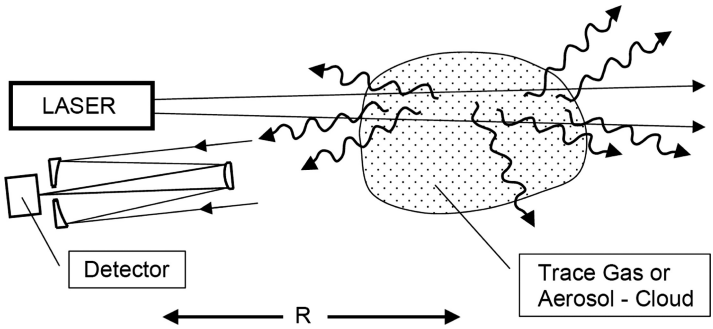

Fig. 1.15 The principle of the lidar technique.

The amout of energy returned is given by the general lidar equation:

$$E(\lambda, R, \Delta R) = K \cdot E_0 \cdot c_S(R)\, \sigma_{SR} \frac{\Delta R}{R^2} \cdot \exp\left(-2 \int_0^R [\sigma_A(r) \cdot c_A(r) + \sigma_S(r) \cdot c_S(r)]\, dr \right) \tag{1.44}$$

where R denotes the distance from which the radiation intensity (under consideration) is scattered back; $R = (c \times t)/2$ where c = speed of light and t = time after emission of the laser pulse at which the signal reaches the detector.

E(λ, R, ΔR) is the radiation energy received from a volume of air between R and R + ΔR where:

ΔR = distance interval to be averaged over (corresponds to $\Delta t = \frac{2\Delta R}{c}$);

K = constant of the system describing the particular properties and size of the receiving system;

E_0 = radiation energy emitted by the LASER;

$c_s(R)$ = concentration of backscattering centres (molecules, aerosol particles)

σ_{SR} = backscatter cross section;

σ_A = absorption cross section (aerosol or gas);
$c_A(R)$ = concentration of absorbers (i.e. gas molecules); and
σ_S = total scattering cross section (note that $\sigma_S \neq \sigma_{RS}$).

Note that here the returned lidar signal is proportional to R^{-2} (Eq. 1.44); in contrast, a returned radar signal varies with R^{-4}. This is due to the fact that the scattering volume for lidar increases with R^2, while in the case of radar the object (e.g. an aircraft) is of constant size and so both the transmitted signal arriving at the target and the returned signal reaching the receiver decrease with R^{-2}.

Lidar techniques have the unique capability of making range-resolved measurements along the line of sight. In the form described so far lidar systems have been successfully used to map aerosol distributions. There are, however, two central problems with lidar systems.

- The signal (Eq. 1.44) depends on the back-scattering as well as on the total scattering (or extinction) properties of the atmosphere. In the case of Mie scattering, these are difficult to separate, since the ratio of σ_S/σ_{SR} is usually unknown and must be estimated from *a priori* information, However if Raman lidar technology is used, the scattering at the Raman wavelength can be corrected with the observed scattering at the excitation wavelength.
- The back scattered signal is usually very weak, so that, even when a high energy laser is used, only a relatively small number of photons are received.

Thus the advantages of the active system are obtained at the expense of sensitivity. However one lidar system, CALIOP, is now being successfully operated in space for aerosol and cloud measurements; for details see Chapter 6 and Appendix A.

a Differential Absorption Lidar (DIAL)

In order to measure the distribution of trace gases at least two different wavelengths are required (Svanberg 1992; Sigrist 1992). The two wavelengths are chosen so that, while the difference in their wavelengths is as small as possible, the difference in the absorption cross sections, $\Delta\sigma = \sigma_A(\lambda_2) - \sigma_A(\lambda_1)$, is as large as possible; normally, one wavelength is at the centre of an absorption line, the other close to the line.

The DIAL equation is obtained by dividing two general lidar equations at two different wavelengths λ_1 and λ_2,

$$\frac{E(\lambda_2,\ R)}{E(\lambda_1,\ R)} = \exp\left(-2(\sigma_A(\lambda_2) - \sigma_A(\lambda_1)) \cdot \int_0^R c_A(r)\, dr\right) \tag{1.45}$$

and it is assumed that σ_{SR} and σ_S are the same for both λ_1 and λ_2, which is justified as long as $\Delta\lambda = \lambda_2 - \lambda_1$ is sufficiently small (a few nm).

The proposed mission, the Water Vapour Lidar Experiment in Space (WALES), will use this technique (Wirth et al. 2009) as will the new Franco-German MERLIN mission.

1.11 Satellite Orbits

The Earth is now orbited by a series of satellites carrying instruments for remote sensing of atmospheric composition. Appendix A summarises the instruments, the spectral ranges used, main species analysed, the type of satellite orbit and other features.

The orbit of the satellite carrying the instrument largely determines its observation capabilities. For instance the "classical" orbit with a small inclination to the equator allows only low latitudes to be probed. A more useful orbit is the polar orbit, which allows the whole earth to be studied. A sun-synchronous orbit always observes the Earth at the same local time during each orbit. In contrast satellites on geo-stationary orbits see only part of the Earth, but they can observe diurnal variations.

1.11.1 Low Earth Orbits (LEO)

In LEO, the satellite circles earth at a relatively low altitude (around 800 km). Sun-synchronous polar orbits are particularly advantageous, where the satellite instrument can observe the whole earth every day or within a few days. The time for the orbit can be adjusted so that the instrument will see the equator at essentially the same local time on each traverse, Fig. 1.16.

In a sun-synchronous orbit the non-sphericity of Earth combined with a small tilt of the orbit (the inclination with respect to the equator) produces a precession so keeping the plane of the orbit at a fixed angle relative to the sun–Earth line. By selecting the inclination of the orbit to the planet's equator, the orbit will precess at the same rate as the planet goes around the sun. For the Earth, the sun-synchronous inclination in LEO is about 98°: it is a retrograde, near-polar orbit, which will always cross the equator at the same local time.

An example of an instrument in a sun-synchronous orbit is provided by the GOME instrument on the ERS-2 satellite; Fig. 1.17. (Burrows et al. 1991; Burrows 1999). The satellite is on a descending orbit crossing the equator at 10.30 a.m. local time. The re-visit time to the same location on the Earth's surface is 3 days.

Sunlight, back-scattered from the Earth, is collected by a scan mirror and then focussed on the entrance slit of a spectrometer, which observes the entire spectral range between 232 and 793 nm with a resolution of between 0.2 nm and 0.33 nm. The instrument is optimised for the collection of the radiation from earth (nadir view) directly by the scan mirror. Fig. 1.18 shows the "whisk broom" scanning scheme used by GOME and other satellite instruments.

The direct, extraterrestrial solar irradiance (the Fraunhofer reference spectrum) is also measured, using a diffuser plate to reduce its intensity prior to it being reflected by the scan mirror into the instrument. The spectra and other signals recorded by GOME are transmitted to the ESA ground station at Kiruna, and then

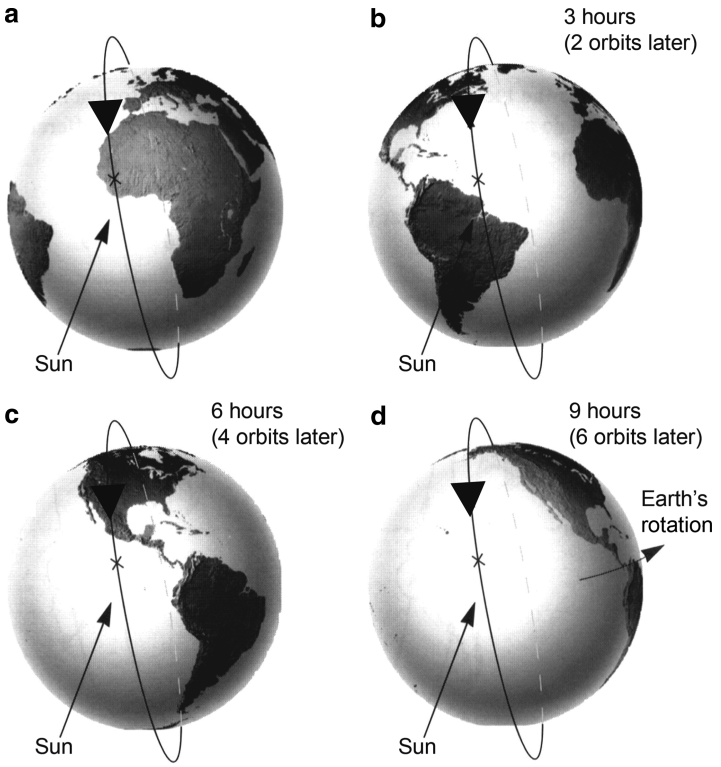

Fig. 1.16 Many satellites circle the Earth on polar orbits (800 km altitude, 100 min per orbit). In a sun synchronous polar orbit, the satellite always crosses the equator at the same local time. Instruments on satellites with these orbits include GOME, SCIAMACHY, AVHRR3, IASI and GOME-2, all of which are all in a descending node traversing from the north to south poles. On the other hand MODIS, OMI and TES are on satellites in an ascending mode. Others are given in Appendix A.

distributed to the waiting laboratories. Details for the other satellite instruments observing the troposphere are given in the table in Appendix A.

1.11.2 Geostationary Orbits (GEO)

Instrumentation placed in the GEO is approximately 36,000 km from the earth and rotates with the earth. As the meteorological observations have demonstrated, this enables optimal temporal sampling and yields diurnal variations. In order to meet the needs of tropospheric chemistry and air quality, a number of missions have been proposed by the community to measure trace gases from a geostationary orbit: for example, the GeoSCIA and GeoFIS instruments and the GeoTROPE concept (Bovensmann et al. 2002; 2004; Burrows et al. 2004).

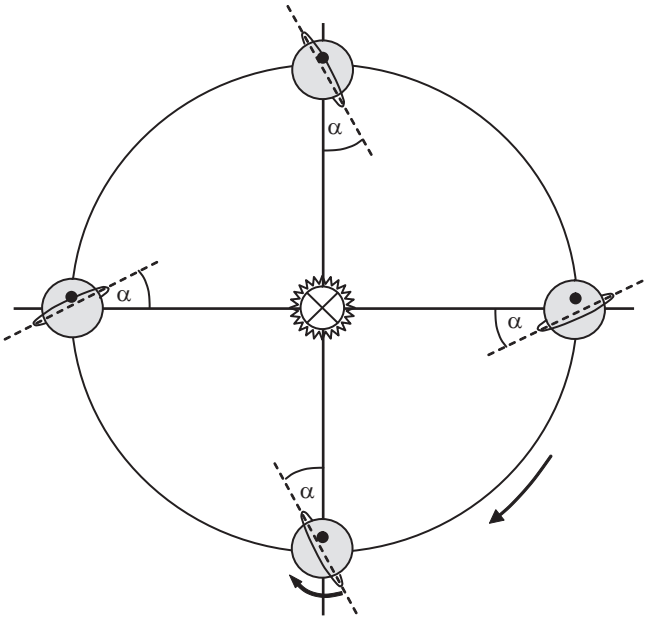

Fig. 1.17 In a sun synchronous polar orbit the satellite always crosses the equator at the same local time. Thus the angle α between the plane of the orbit and the direction towards the sun stays constant, i.e. the plane of the orbit makes a full rotation once a year. The required change in angular momentum is supplied by gravitational forces due to the "equator bulge" of Earth.

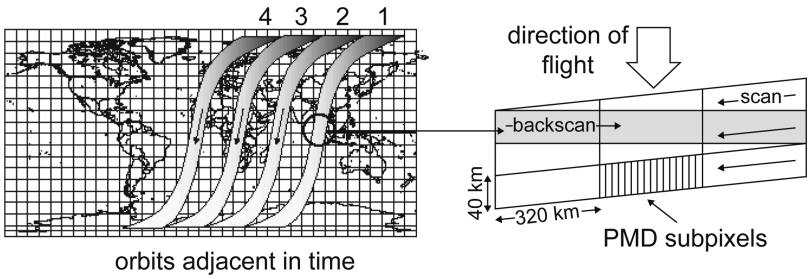

Fig. 1.18 Whisk broom scanning scheme of the GOME instrument. Left panel: Subsequent satellite orbits (numbered 1. . .4) on a world map. Right panel: Each scan consists of three ground pixels plus one "back-scan pixel". Later instruments (SCIAMACHY, GOME-2) divide a scan into more pixels. Fig. from Leue et al. (2001).

Based on this innovative work Europe has now decided, as part of its Meteosat Third Generation and GMES Sentinel 4 programmes, to fly a UVN and an IRS instrument, which meet some of the objectives of the GeoTROPE mission.

A full list of satellite instruments for observing tropospheric chemical composition with solar back-scattered radiation is given in Appendix A.

1.12 Summary

This chapter has provided the historical highlights in the development of tropospheric remote sounding from space, which is now an essential part of the modern science of Earth observation. The scientific background required to understand why the remote sounding of trace constituents is important and how it has evolved has been presented, together with an introduction to the approaches needed to retrieve trace gases, cloud and aerosol parameters. The following chapters expand on these topics and present the remarkable results that have been obtained so far. Some outlines of future needs and activities are given in the concluding chapter, Chapter 10.

References

Angström A., 1929, On the atmospheric transmission of sun radiation and on dust in the air, *Geogr. Ann.* Stockholm **11**, 156–166.

Arrhenius S., 1896, On the influence of carbonic acid in the air upon the temperature of the ground, *The London, Dublin, and Edinburgh Philosophical Magazine and Journal of Science* **41**, 237–276.

Barrie L.A., Bottenheim J.W., R.C. Shnell, P.J. Crutzen and Rasmussen R.A., 1988, Ozone destruction and photochemical reactions at polar sunrise in the lower Arctic atmosphere, *Nature* **334**, 138–141.

Barrie, L.A., P. Borrell and J. Langen, 2004, The Integrated Global Atmospheric Chemistry Observations Theme (IGACO) Report on Monitoring of our Environment from Space and from Earth, European Space Agency (ESA) SP1235; Global Atmospheric Watch (GAW) 159, *World Meteorological Organisation (WMO) TD* 1235, pp 54.

Bone N., 1991, The Aurora: Sun–Earth Interactions, Ellis Horwood, Chichester.

Borrell P, Borrell P.M., Burrows J.P., and Platt U. (Eds.), 2003, Sounding the Troposphere from Space: a new Era for Atmospheric Chemistry, The TROPOSAT Final Report, Springer Verlag, Heidelberg, 446 pp.

Brekke A. and Egeland A., 1994, The northern lights: their heritage and science, Grøndahl Dreyer, ISBN-13: 9788250421059 ISBN: 8250421051.

Bovensmann, H., J. P. Burrows, M. Buchwitz, J. Frerick, S. Noël, V. V. Rozanov, K. V. Chance, A. P. H. Goede, 1999, "SCIAMACHY- mission objectives and measurement modes", *Atmos Sci* 56 127–150.

Bovensmann H., S. Noel, P. Monks, A.P.H. Goede, J.P. Burrows, 2002, The Geostationary Scanning Imaging Absorption Spectrometer (GEOSCIA) Mission: Requirements and Capabilities, *Adv. Space Res.*, 29(11), pp 1849–1859.

Bovensmann H., K. U. Eichmann, S. Noel, J. M. Flaud, J. Orphal, P.S. Monks, G. K. Corlett, A. P. Goede, T, von Clarmann, T. Steck, V. Rozanov and J. P. Burrows, 2004, The Geostationary scanning imaging absorption spectrometer (GeoSCIA) as part of the Geostationary pollution exlorer (GeoTROPE) mission: requirements concepts and capabilities. *Adv. Space Research* **34**(2004) 694–699.

Burrows J. P., W. Schneider, J. C. Geary, K. V. Chance, A. P. H. Goede, H. J. M. Aarts, J. de Vries, C. Smorenburg and H. Visser, 1990, "Atmospheric remote sensing with SCIAMACHY.", Digest of Topical Meeting on Optical Remote Sensing of the Atmosphere 1990 (Optical Society of America, Washington D.C. 1990) 4 71 1990.

Burrows J. P., E. Hölzle, A. P. H. Goede, H. Visser and W. Fricke, 1995, "SCIAMACHY - Scanning Imaging Absorption Spectrometer for Atmospheric Chartography." *Acta Astronautica* **35(7)** 445–451

Burrows J.P., 1999, "Current and future passive remote sensing techniques used to determine atmospheric constituents", in *Developments in Atmospheric Sciences* **24**: Approaches to Scaling Trace Gas Fluxes in Ecosystems, Ed A. F. Bouwman Elservier Amsterdam pp 315–347. ISBN: 0-444-82934-2.

Burrows J.P., Chance K.V., Crutzen P.J., Fishman J., Fredericks J.E., Geary J.C., Johnson T.J., Harris, G.W., Isaksen I.S.A., Kelder H., Moortgat G.K., Muller C., Perner D., Platt, U., Pommereau J.-P., Rodhe H., Roeckner E., Schneider W., Simon P., Sundqvist H., Vercheval J., 1991, SCIAMACHY Phase A Study – *Scientific Requirements Specification.*

Burrows J.P., Weber M., Buchwitz M., Rozanov V., Ladstätter-Weißenmayer A., Richter A., DeBeek, R., Hoogen R., Bramstedt K., Eichmann K. -U., Eisinger M., and Perner D., 1999, The Global Ozone Monitoring Experiment (GOME): Mission Concept and First Scientific Results, *J. Atmos. Sci.* **56**, 151–171.

Burrows J.P., H. Bovensmann, G. Bergametti, J.M. Flaud, J. Orphal, S. Noel, P.S. Monks, G.K. Corlett, A.P. Goede, T. v. Clarmann, T. Steck, H. Fischer, F. Friedl-Vallon, 2004, The geostationary tropospheric pollution explorer (GeoTROPE) missions: objects, requirements and mission concept, *Adv. Space Research*, **34**, 682–687, doi. 10.1016/j.asr. 2003.08.067.

Chapman S., 1930, On ozone and atomic oxygen in the upper atmosphere, *Phil. Mag*. **S7**, 369–383.

Climate Change 2007 – Impacts, Adaptation and Vulnerability, Contribution of Working Group II to the Fourth Assessment Report of the IPCC, (978 0521 88010-7 Hardback; 978 0521 70597-4 Paperback).

Climate Change 2007 – Mitigation of Climate Change, Contribution of Working Group III to the Fourth Assessment Report of the IPCC, (978 0521 88011-4 Hardback; 978 0521 70598-1 Paperback). Climate Change 2007 – Synthesis Report.

Crutzen P.J., 1973, A discussion of the chemistry of some minor constituents in the stratosphere and troposphere, *Pure Appl. Geophys.* **106,** 1385–1399.

Crutzen P.J., 1974, Photochemical reactions initiated by and influencing ozone in unpolluted tropospheric air, *Tellus* **26**, 47–57.

Crutzen P.J. and Andreae M.O., 1990, Biomass burning in the tropics: Impact on atmospheric chemistry and biogeochemical cycles, *Science* **250**, 1669–1678.

Crutzen P.J., and Stoermer E.F., 2000, The "Anthropocene". *Global Change Newsletter*. **41**: 17–18.

Dameris M., Grewe V., Hein R., Schnadt C. Brühl C., and Steil B., 1998, Assessment of the future development of the ozone layer, *Geophys. Res. Lett*. **25 (19)**, 3579–3582.

Einstein, A., 1917 Zur Quantentheorie der Strahlung, *Phys Z.*, **18**, 121–128.

Farman J.C., Gardiner B.G., Shanklin J.D., 1985, Large losses of total ozone in Antarctica reveal seasonal ClO_X/NO_x interaction, *Nature* **315**, 207–210.

Finlayson-Pitts B.J. and Pitts J.N., 1986, Chemistry of the Upper and Lower Atmosphere: Theory, Experiments, and Applications, Academic Press, 1st edition (November 1999), 969 pp., ISBN-10: 012257060X, ISBN-13: 978-0122570605, and references therein.

Fischer H. and Oelhaf H., 1996, Remote sensing of vertical profiles of atmospheric trace constituents with MIPAS limb emission spectrometers, *Applied Optics* **35 (16)**, 2787–2796.

Fishman, J., C.E. Watson, J.C. Larsen and J.A. Logan, 1990, Distribution of tropospheric ozone determined from satellite data. *J. Geophys. Res.,* **95**:3599–3617.

Fleming J.R., 1998, Historical Perspectives on Climate Change. Oxford University Press, New York, 208pp.

Funk O., 2000, Photon path length distributions for cloudy skies; oxygen a-band measurements and radiative transfer calculations, Doctoral Thesis, University of Heidelberg, Heidelberg, Germany.

GEOSS 2009, The Global Earth Observation System of Systems, http://earthobservations.org/

Gottwald M., Bovensmann H., (eds.), 2010, SCIAMACHY - Exploring the Changing Earth's Atmosphere. Springer Heidelberg, ISBN: 978-90-481-9895-5, doi: 10.1007/978-90-481-9896-2.

Grannas A.M., Jones A.E., Dibb J., Ammann M., Anastasio C., Beine H.J., Bergin M., Bottenheim J., Boxe C.S., Carver G., Chen G., Crawford J.H., Dominé F., Frey M.M., Guzmán M.I., Heard D.E., Helmigh D., Hoffmann M.R., Honrath R.E., Huey L.G., Hutterli M., Jacobi H.W., Klán P., Lefer B., McConnell J., Plane J., Sanders R., Savarino J.,

Shepson P.B., Simposon W.R., Sodeau J.R., von Glasow R., Weller R., Wolff E.M.and Zhu T., 2007, An overview of snow photochemistry: evidence, mechanisms and impacts, *Atmos. Chem. Phys.* **7**, 4329–4373.

Haagen-Smit A.J., 1952, Chemistry and physiology of Los Angeles smog, *Ind. Engin. Chem.* **44**, 1342–1346.

Haagen-Smit, A.J., Darley, E.F., Zailin, M., Hull, H., and Noble, W., 1952, Investigation on injury to plants from air pollution in the Los Angeles area. *Plant Physiology* **27**:18.

Heath D.F., Mateer C. L. and Krueger A. J., 1973, The Nimbus -4 Backscatter Ultraviolet (BUV) Atmospheric Ozone Experiment – Two Years of Operation, *Pure and Applied Geophysics* **106–108** 1238–1253.

Heath D.F., Krueger A.J, Roeder H.A., and Henderson B.D., 1975, "The Solar backscatter Ultraviolet and the Total Ozone Mapping Spectrometere (SBUV/TOMS) for Nimbus G. *Opt. Eng.* **14** 323–332

Heij G.J. and Erisman J.W. (Eds.) 1995, Acid rain research: Do We Have Enough Answers?, Elsevier, Amsterdam, 502pp., ISBN 0-444-82038-9.

Herzberg, G., 1950, Spectra of Diatomic Molecules, van Nostrand, New York.

Hinkley E.D. (Ed.) 1976, Laser Monitoring of the Atmosphere, Topics in Appl. Physics, Vol. 14, Springer Berlin, Heidelberg.

Holloway, A.M. and Wayne, R.P., 2010, Atmospheric Chemistry, Royal Society of Chemistry, London, ISBN 9781847558077.

Horowitz, L.W., 2006, Past, present, and future concentrations of tropospheric ozone and aerosols: Methodology, ozone evaluation, and sensitivity to aerosol wet removal. *J. Geophys. Res.* **111** (D22), D22211.

HTAP 2007, Hemispheric Transport of Air Pollution 2007, Air Pollution Studies No. 16, Interim report prepared by the Task Force on Hemispheric Transport of Air Pollution acting within the framework of the Convention on Long-range Transboundary Air Pollution, Economic Commission for Europe, Geneva, United Nations, New York and Geneva, 2007

IPCC 4th Assessment Report, 2007 available at http://www.ipcc.ch/Climate Change 2007 and comprising the elements: The Physical Science Basis. Contribution of Working Group I to the Fourth Assessment Report of the IPCC, (ISBN 978 0521 88009-1 Hardback; 978 0521 70596-7 Paperback).

Isaacs, R. G., W.-C. Wang, R. D. Worsham, and S. Goldberg, 1987. Multiple Scattering Lowtran and Fascode models. *Appl.* Opt. **26**, 1272–1281.

Janssen M.A. (1993), An Introduction to the Passive Remote Atmospheric Remote Sensing by Microwave Radiometry, J. Wiley & Sons Inc., New York, pp.1–36.

Kahn, R.A. W.H. Li, C. Moroney, D. J. Diner, J. V. Martonchik, and E. Fishbein, 2007 Aerosol source plume physical characteristics from space-based multiangle imaging, *J. Geophys. Res.*, **112**, D11205, doi:10.1029/2006JD007647

Kahn, R., A. Petzold, M. Wendisch, E. Bierwirth, T. Dinter, M. Esselborn, M. Fiebig, B. Heese, P. Knippertz, D. Műller, A. Schladitz and W. von Hoyningen-Huene, 2008 Desert dust aerosol air mass mapping in the western Sahara, using particle properties derived from space-based multi-angle imaging. *Tellus* **61**, 239–251. Doi:10.1111/j.1600-0889.2008.00398.x

Keeling C.D., Barcastow R.B., Bainbridge A.E., Ekdahl C.A., Guenther P.R., Waterman L.S., 1976, Atmospheric carbon dioxide variations at Mauna Loa observatory, Hawaii, *Tellus* **28,** 538–551.

Keeling, R.F., S.C. Piper, A.F. Bollenbacher and J.S. Walker, 2003, CDIAC, DOI: 10.3334/CDIAC/atg.035

Klein U., Wohltmann I., Lindner K., and Künzi K.F., 2002, Ozone depletion and chlorine activation in the Arctic winter 1999/2000 observed in Ny-Ålesund, *J. Geophys. Res.* **107(D20)**, 8288, doi:10.1029/2001JD000543.

Le Treut, H., R. Somerville, U. Cubasch, Y. Ding, C. Mauritzen, A. Mokssit, T. Peterson and M. Prather (2007), Historical Overview of Climate Change. In: Climate Change 2007: The Physical Science Basis. Contribution of Working Group I to the Fourth Assessment Report of the Intergovernmental Panel on Climate Change.

Leue C., Wenig M., Wagner T., Platt U. and Jähne B., 2001, Quantitative analysis of NOX emission from Global Ozone Monitoring Experiment satellite image sequences, *J. Geophys. Res.* **106**, 5493–5505.

Levine J.S., 1991, Global Biomass Burning: Atmospheric, Climatic, and Biospheric Implications. MIT Press, Cambridge, MA.

Livesey N.J., Read W.G., Froidevaux L., Waters J.W., Santee M.L., Pumphrey H.C., Wu D.L., Shippony Z., and Jarnot R.F., 2003, The UARS Microwave Limb Sounder version 5 data set: Theory, characterization, and validation, *J. Geophys. Res.* **108(D13)**, 4378, doi:10.1029/2002JD002273.

Lovelock J.E., Maggs R.J., and Wade R.J., 1973, Halogenated hydrocarbons in and over the Atlantic, Nature **241**, 194–196.

LRTAP 2004, Handbook for the 1979 Convention on Long-range Transboundary Air Pollution and its protocols, United Nations, New York and Geneva. (see also: http://www.unece.org/env/lrtap/welcome.html)

Martonchik, J.V., D. J. Diner, B. Pinty, M. M. Verstraete, R. B. Myneni, Y. Knyazikhin, H. R. Gordon, 1998, Determination of land and ocean reflective, radiative, and biophysical properties using multiangle imaging, http://citeseerx.ist.psu.edu/viewdoc/summary? doi: 10.1.1.32.5688

Mie, Gustav, 1908, Beiträge zur Optik trüber Medien, speziell kolloidaler Metallösungen, *Annalen der Physik, Vierte Folge,* Band **25, No. 3,** 377–445.

Molina, M.J. and Rowland, F.S., 1974, Stratospheric sink for chlorofluoromethanes: chlorine atomc-catalysed destruction of ozone, *Nature* **249**, 810–812; doi:10.1038/249810a0

Nicolet M., 1984, On the Molecular Scattering in the Terrestrial Atmosphere: An Empirical Formula for its Calculation in the Homosphere. *Planet. Space Sci.* **32**(11) 1467–1468.

Noxon J.F., 1975, Nitrogen dioxide in the stratosphere and troposphere measured by ground-based absorption spectroscopy, *Science* **189**, 547–549

O'Dowd, C. D., Geever, M., and Hill, M. K. (1998), New particle formation: Nucleation rates and spatial scales in the clean marine coastal environment, *Geophys. Res. Lett.*, **25(10)**, 1661–1664.

O'Dowd, C. D., Jimenez, J. L., Bahreini, R., Flagan, R. C., Seinfeld, J. H., Hameri, K., Pirjola, L., Kulmala, M., Jennings, S. G., and Hoffmann, T., 2002, Marine aerosol formation from biogenic iodine emissions, *Nature,* **417,** 632–636.

Penndorf R., 1957, Tables of the refractive index for standard air and the Rayleigh scattering coefficient for the spectral region between 0.2 and 20.0 μ and their application to atmospheric optics, *J. Opt. Soc. Amer.* **47**, 176–182.

Perner D. and Platt U., 1979, Detection of nitrous acid in the atmosphere by differential optical absorption, *Geophys. Res. Lett.* **6**, 917–920.

Platt U. and Lehrer E., (Eds.) 1996, Arctic Tropospheric Halogen Chemistry, *Final Report to EU*.

Platt U., Pfeilsticker K. and Vollmer M., 2007, Radiation and Optics in the Atmosphere, Ch. 19 in: "Springer Handbook of Lasers and Optics", F. Träger Ed., Springer, Heidelberg, ISBN-10: 0-387-95579-8, pp. 1165–1203.

Platt, U. and J. Stutz, 2008, Differential optical absorption spectroscopy: principles and applications, Springer Verlag, Heidelberg, ISBN 978-3540211938, pp597.

Pommereau, J.P., 1982, First balloon flight of vis spectrometer for NO2. Observation of NO_2 diurnal variation in the stratosphere, *Geophys. Res. Lett.*, 850.

Pommereau, J.P. and J. Piquard, 1994a, First publications relative to SAOZ balloon flights in Kiruna, Ozone. Nitrogen dioxide and Aerosol vertical distributions by UV-visible solar occultation from balloons, *Geophys. Res. Lett,* **21**, 1227–1230.

Pommereau, J.P. and J. Piquard, 1994b, Observations of the vertical distribution of stratospheric OClO, *Geophys. Res. Lett.*, **21**, 1231–1234.

Rayleigh, Lord, 1899, On the transmission of light through an atmosphere containing many small particles in suspension, and on the origin of the blue of the sky, *Phil. Mag.* **41**, 447–454. Also: in 'the scientific papers of Lord Rayleigh', Vol. 4, Dover, New York, 1964.

Ravishankara, A.R., J.S. Daniel and R.W. Portmann. 2009, Nitrous Oxide (N_2O): The dominant ozone-depleting substance emitted in the 21st century Published online 31 August 2009. DOI: 10.1126/science.1176985

Roach, F.E.and Gordon J.L., 1973, The Light of the Night Sky, Reidel, Dordrecht.

Rothe, K.W., Brinkmann U., Walther H., 1974, Applications of tunable dye lasers to air pollution detection: Measurements of atmospheric NO_2 concentrations by differential absorption, *Appl. Phys.* **3**, 115–119.

Schär C. and Jendritzky G., 2004, Hot news from summer 2003, *Nature* **432**, 559–560.

Schär C., Vidale P.L., Lüthi D., Frei C., Häberli C., Liniger M.and Appenzeller C., 2004, The role of increasing temperature variability for European summer heat waves, *Nature* 427, 332–336.

Seinfeld, J.H., S.N. Pandis, 1998, Atmospheric Chemistry and Physics, from Air Pollution to Climate Change, *J. Atmos. Chem.*, **37**, 212–214.

Shindell D.T., Rind D. and Lonergan P., 1998, Increased polar stratospheric ozone losses and delayed eventual recovery owing to increasing greenhouse-gas concentrations. *Nature* **392**, 589–592, doi:10.1038/33385.

Sigrist M.W. (Ed.) 1994, Air monitoring by spectroscopic techniques, *Chemical Analysis Series,* Vol. **127,** John Wiley & Sons, Inc.

Simpson W.R., R. von Glasow, K. Riedel, P. Anderson, P. Ariya, J. Bottemheim, J. Burows, L. J. Carepnter, U. Frieß, M. Goodsite, D. Heard, M. Hutterli, H.-W. Jacobi, L. Kaleschke, B. Neff, J. Plane, U. Platt, A. Richter, H. Roscoe, R. Sander, P. Shepson, J. Sodeau, A. Stefann, T. Wagner and E. Wolff, 2007, Halogens and their role in polar boundary-layer ozoen depletion, *Atmos Chem. Phys.* **7**, 4375–4418.

Steffan A., Douglas T., Amyot M., Ariya P., Aspmo K., Berg T., Bottenheim J., Brooks S., Corbett F., Dastoo A., Dommergue A., Ebinghaus R., Ferrari C., Gardefeldt K., Goodsite M.E., Lean D., Poulain A.J., Scherz C., Skov H., Sommar J.and Temme C., 2008, A synthesis of atmospheric mercury depletion event chemistry in the atmosphere and snow, *Atmos. Chem. Phys.* **8**, 1445–1482.

Svanberg S., 1992, Atomic and Molecular Spectroscopy, 2nd Edition, Springer Series on Atoms and Plasmas, Springer Berlin, Heidelberg.

U.S. Standard Atmosphere, 1976, U.S. Government Printing Office, Washington, D.C.

Van de Hulst, H.C., 1980, Multiple Light Scattering, Tables, Formulas and Applications, Volume 1 and 2. London: Academic Press.

Volz A. and Kley D., 1988, Ozone Measurements in the 19th century: An Evaluation of the Montsouris series, *Nature* **332**, 240–242.

Wang J., Zhang X., Keenan T. and Duan Y., 2009, Air-quality management and weather prediction during the 2008 Beijing Olympics, *WMO Bulletin* **58 (1),** 31–40.

Watson, C.E.; Fishman, J.; Reichle, H.G.Jr., 1990, The significance of biomass burning as a source of carbon monoxide and ozone in the southern hemisphere tropics: A satellite analysis, *J. Geophy. Res.,* **95 (D10),** 16,443–16, 450.

Wayne, R.P. (2000), Chemistry of atmospheres (3rd Ed.). Oxford University Press. ISBN 0-19-850375-X

Weart, S., (2003), The Discovery of Global Warming. Harvard University Press, Cambridge, MA, 240 pp.

Wirth M., Fix A., Mahnke P., Schwarzer H., Schrandt F., and Ehret G., 2009, The airborne multi-wavelength water vapour differential absorption lidar WALES: system design and performance. *App. Phys. B-Lasers & Optics*, **96**, 201–213.

Wiscombe, W. J. (1980). Improved Mie scattering algorithms. *Appl. Op*t. **19**, 1505–1509.

WMO (World Meteorological Organization) 2007, Scientific Assessment of Ozone Depletion: 2006, *Global Ozone Research and Monitoring Project—Report* **50**, 572 pp., Geneva, Switzerland.